
PRESENTATION OF THE NEPTUNE_CFD CODE

Contents

1.1	Introduction	3
1.2	Governing Equations for Turbulent Boiling Bubbly Flows	3
1.2.1	Mass Conservation	4
1.2.2	Momentum Balance	4
1.2.3	Energy Conservation	4
1.3	Interfacial Transfers Closure Laws	4
1.3.1	Heat and Mass Transfers	4
1.3.2	Interfacial Forces	6
1.4	Turbulence Modeling	7
1.5	Wall Boiling Model	8
1.6	Wall Function for Dispersed Boiling Flows	9

1.1 INTRODUCTION

The NEPTUNE_CFD project (started in 2001) is a research program coordinated by four entities : EDF, CEA, IRSN and Framatome. The initial goals of the project were related to nuclear safety by developing a thermal-hydraulics simulation tool to :

- Predict the Boiling Crisis in PWR cores ;
- Study the Loss Of Coolant Accident (LOCA) to predict fuel rod cladding temperature.

As a multiphase eulerian code, NEPTUNE_CFD consists of a local three-dimensional modeling based on a two fluids-one pressure approach combined with mass, momentum and energy conservation equations for each phase [45].

The constitutive equations are solved using a pressure correction and is based on a finite-volume discretization along with a collocated arrangement of the variables. Moreover, NEPTUNE_CFD allows the use of all type of meshes (hexahedra, tetrahedra, pyramids, etc.), even non-conforming ones, thanks to its face-based data structure. Finally, the code is well-suited for parallel computing, widening its computing capacity to very large meshes.

The simulations presented in this thesis have all been conducted using the NEPTUNE_CFD 7.0 modeling framework for dispersed bubbly flows. In the next sections, we will detail the constitutive equations and physical modeling of the code for the simulation of boiling bubbly flows.

1.2 GOVERNING EQUATIONS FOR TURBULENT BOILING BUBBLY FLOWS

To simulate two-phase dispersed boiling flows, NEPTUNE_CFD solves the ensemble-averaged equations of mass conservation, momentum balance and energy conservation for each phase (see Ishii [52] for details on the derivation).

1.2.1 Mass Conservation

$$\frac{\partial \alpha_k \rho_k}{\partial t} + \bar{\nabla} \cdot (\alpha_k \rho_k \bar{U}_k) = \Gamma_k \quad (1.1)$$

Where α_k , ρ_k , \bar{U}_k are the time fraction, average density and velocity of phase k ; $\Gamma_k = \Gamma_{k,i} + \Gamma_{k,w}$ the interfacial mass transfer term per unit of volume and time splitted between bulk and wall contribution. Subscripts $k = L$ or V denotes the liquid or vapor phase, i the interfacial quantities and w the wall contribution.

1.2.2 Momentum Balance

$$\frac{\partial \alpha_k \rho_k \bar{U}_k}{\partial t} + \bar{\nabla} \cdot (\alpha_k \rho_k \bar{U}_k \otimes \bar{U}_k) = -\alpha_k \bar{\nabla} (P) + \bar{F}_{k,i} + \Gamma_k \bar{U}_{k,i} + \alpha_k \rho_k \bar{g} + \bar{\nabla} \cdot (\alpha_k (\bar{\tau}_{k,m} + \bar{\tau}_{k,T})) \quad (1.2)$$

Where P is the pressure, \bar{g} the gravity, $\bar{F}_{k,i}$ the interfacial forces accounting for momentum transfer between phases per unit of volume and time, $\bar{U}_{k,i}$ the interfacial velocity, $\bar{\tau}_{k,m}$ and $\bar{\tau}_{k,T}$ respectively the viscous and turbulent (or Reynolds) stress tensor. Subscript m and T respectively denote the molecular (or laminar) and turbulent terms.

1.2.3 Energy Conservation

$$\begin{aligned} \frac{\partial \alpha_k \rho_k H_k}{\partial t} + \bar{\nabla} \cdot (\alpha_k \rho_k H_k \bar{U}_k) &= \frac{\partial \alpha_k P}{\partial t} + \Gamma_k H_{k,i} + \bar{F}_{k,i} \cdot \bar{U}_k + \bar{Q}_{k,I} + \bar{\nabla} \cdot (\alpha_k (\bar{\tau}_k + \bar{\tau}_{k,T}) \cdot \bar{U}_k) \\ &\quad + \bar{\nabla} \cdot (\alpha_k (-(\lambda_{k,m} + \lambda_{k,T}) \bar{\nabla} (T_k))) + \alpha_k \rho_k \bar{g} \cdot \bar{U}_k + \bar{Q}_{k,w} \end{aligned} \quad (1.3)$$

Where $H_k = e_k + \frac{U_k^2}{2} + \frac{P}{\rho_k} = h_k + \frac{U_k^2}{2}$ is the total enthalpy of phase k , $H_{k,i}$ the interfacial-averaged enthalpy, $\bar{Q}_{k,i}$ the interfacial heat flux per unit of volume and time, $\lambda_{k,m}$ and $\lambda_{k,T}$ respectively being the laminar and turbulent thermal conductivity, T_k the temperature, $\bar{Q}_{k,w}$ the heat flux from the wall to phase k per unit of volume and time.

The viscous and Reynolds stress tensors read:

$$\bar{\tau}_{k,m} = \mu_k \left(\bar{\nabla} (\bar{U}_k) + \bar{\nabla} (\bar{U}_k)^T - \frac{2}{3} \bar{\nabla} \cdot (\bar{U}_k) \bar{I} \right) \quad (1.4)$$

$$(\bar{\tau}_{k,T})_{i,j} = -\rho_k \left\langle U'_{k,i} U'_{k,j} \right\rangle_k \quad (1.5)$$

with \bar{U}'_k is the fluctuating part of velocity for phase k .

This ensemble-average approach requires a given number of closure laws since this mathematical averaging operation removes most of the information about smaller scales physics (compared to the mesh size) such as interfacial exchanges between phases or wall-fluid interaction. Terms for which this modeling effort is needed are colored in orange in equations 1.1, 1.2 and 1.3. Following sections detail the physical modeling for each of those terms.

1.3 INTERFACIAL TRANSFERS CLOSURE LAWS

The interfacial transfers of mass, momentum and energy are respectively noted in equations 1.1, 1.2 and 1.3 : Γ_k , $\bar{F}_{k,i}$ and $\bar{Q}_{k,i}$.

1.3.1 Heat and Mass Transfers

The mass transfer term, can be written as:

$$\Gamma_{L,i} + \Gamma_{V,i} = 0 \quad (1.6)$$

$$\Gamma_{L,w} + \Gamma_{V,w} = 0 \quad (1.7)$$

with $\Gamma_{V,w} \geq 0$ in the case of boiling flows. This finally gives:

$$\Gamma_L = -\Gamma_V \quad (1.8)$$

The interfacial heat flux $Q_{k,i}$ can be rewritten in terms of interfacial area concentration a_i :

$$Q_{k,i} = q''_{k,i} a_i \quad (1.9)$$

Neglecting the mechanical contribution compared to the thermal terms, the energy jump condition can then be expressed as :

$$\sum_{k=L,V} \left(\Gamma_{k,i} h_{k,i} + q''_{k,i} a_i \right) = 0 \quad (1.10)$$

The estimation of $h_{k,i}$ is not straightforward since it can either be supposed as:

- H1) The saturation enthalpy of phase k at the system pressure ;
- H2) The phase-averaged enthalpy.

In NEPTUNE_CFD, the assumption H2 is chosen, thus giving the bulk condensation rate :

$$\Gamma_{L,i} = \frac{a_i (q''_{L,i} + q''_{V,i})}{h_V - h_L} \quad (1.11)$$

The interfacial heat flux densities $q''_{k,i}$ and interfacial area concentration a_i are expressed as:

$$q''_{k,i} = C_{k,i} (T_{sat}(P) - T_k) \quad (1.12)$$

$$a_i = 6\alpha_V / D_V \quad (1.13)$$

with D_V being the vapor phase Sauter mean bubble diameter and $C_{k,i}$ the interfacial heat transfer coefficient.

Note : The interfacial area is computed using the transport equation of Ruyer & Seiler [103].

1.3.1.1 Subcooled Liquid

For subcooled liquid, the following heat transfer coefficient is used [79, 96]:

$$C_{L,i} = \frac{\text{Nu}_L \lambda_L}{d_G} \quad (1.14)$$

$$\text{Nu}_L = 2 + 0.6 \text{Re}_b^{1/2} \text{Pr}_L^{1/3} \quad (1.15)$$

Where Re_b is the bubble Reynolds number $\text{Re}_b = \frac{|\overline{U}_V - \overline{U}_L| D_V}{\nu_L}$ and $\text{Pr}_L = \frac{\nu_L}{\eta_L}$ the liquid Prandtl number with ν_L and η_L respectively being the liquid kinematic viscosity and thermal diffusivity.

1.3.1.2 Superheated Liquid

On the other hand, if the liquid is overheated, the maximum of three heat transfer coefficients accounting for different heat transfer mechanisms is taken [5]:

$$C_{L,i} = \max (C_{L,i,1} ; C_{L,i,2} ; C_{L,i,3}) \quad (1.16)$$

With $C_{L,i,n} = \frac{\lambda_L \text{Nu}_{L,n}}{D_V}$ and :

$$Nu_1 = \sqrt{\frac{4}{\pi} Pe} ; Nu_2 = 2 ; Nu_3 = \frac{12}{\pi} Ja_L \quad (1.17)$$

where $Pe = Re_b Pr_L$ is the Peclet number, $Ja_L = \frac{\rho_L c_{p,L} |T_{sat} - T_L|}{\rho_V h_{LV}}$ the liquid Jakob number and h_{LV} the latent heat of vaporization.

Those three Nusselt numbers respectively correspond to convective heat transfer, stationnary conduction and transient conduction.

1.3.1.3 Vapor Heat Transfer

For the vapor phase, a simple law that ensures the vapor temperature to stay close to the saturation temperature is used (which is expected for small bubbles, *e.g.* in a PWR) :

$$C_{V,i} a_i = \frac{\alpha_V \rho_V c_{p,V}}{t_c} \quad (1.18)$$

where $c_{p,V}$ is the vapor heat capacity at constant pressure and t_c a characteristic (relaxation) time given by the user (default value being $t_c = 0.01$ s) .

1.3.2 Interfacial Forces

The interfacial momentum transfer (excluding transfer associated to transfer of mass Γ_k) is assumed to be composed of 4 different forces being the, drag D , the added mass AM , the lift L and the turbulent dispersion TD :

$$\overline{F_{k,i}} = \overline{F_{k,D}} + \overline{F_{k,AM}} + \overline{F_{k,L}} + \overline{F_{k,TD}} \quad (1.19)$$

The turbulent dispersion force $\overline{F_{k,TD}}$ originates from the averaging operation conducted on the three other forces expressions, detailed in equations 1.20, 1.24, 1.25 and 1.28.

1.3.2.1 Drag Force

The drag force is modeled according to Ishii & Zuber [53]:

$$\overline{F_{V,D}} = -\overline{F_{L,D}} = -\frac{1}{8} a_i \rho_L C_D \left| \overline{U_V} - \overline{U_L} \right| (\overline{U_V} - \overline{U_L}) \quad (1.20)$$

$$C_D = \frac{2}{3} D_V \sqrt{\frac{g(\rho_L - \rho_V)}{\sigma}} \left(\frac{1 + 17.67 f(\alpha)^{1.67}}{18.67 f(\alpha)} \right), \quad f(\alpha) = (1 - \alpha)^{1.5} \text{ for distorted bubbles.} \quad (1.21)$$

$$C_D = \frac{8}{3} (1 - \alpha)^2 \text{ for churn-turbulent regime.} \quad (1.22)$$

1.3.2.2 Added Mass Force

The added mass force is modeled following Zuber [137]:

$$\overline{F_{V,AM}} = -\overline{F_{L,AM}} = -C_{AM} \frac{1 + 2\alpha_V}{1 - \alpha_V} \alpha_V \rho_L \quad (1.23)$$

$$\times \left[\left(\frac{\partial \overline{U_V}}{\partial t} + \overline{\nabla}(\overline{U_V}) \cdot \overline{U_V} \right) - \left(\frac{\partial \overline{U_L}}{\partial t} + \overline{\nabla}(\overline{U_L}) \cdot \overline{U_L} \right) \right] \quad (1.24)$$

with $C_{AM} = \frac{1}{2}$ and the term $\frac{1 + 2\alpha_V}{1 - \alpha_V}$ accounts for the impact of bubble concentration.

1.3.2.3 Lift Force

The lift force is modeled based on the experiments of Tomiyama *et al.* [120]:

$$\overline{F_{V,L}} = -\overline{F_{L,L}} = -C_L \alpha_V \rho_L (\overline{U_V} - \overline{U_L}) \wedge (\nabla \wedge \overline{U_L}) \quad (1.25)$$

$$C_L = \begin{cases} \min(0.288 \tanh(0.121 \text{Re}_b) ; 0.00105 \text{Eo}_H^3 - 0.0159 \text{Eo}_H^2 - 0.0204 \text{Eo}_H + 0.474), & \text{if } \text{Eo}_H < 4 \\ 0.00105 \text{Eo}_H^3 - 0.0159 \text{Eo}_H^2 - 0.0204 \text{Eo}_H + 0.474, & \text{if } 4 \leq \text{Eo}_H \leq 10 \\ -0.27, & \text{if } \text{Eo}_H > 10 \end{cases} \quad (1.26)$$

where $\text{Eo}_H = \frac{g(\rho_V - \rho_L) D_H^2}{\sigma}$ is a modified Eötvös number with:

$$D_H = D_V \sqrt[3]{1 + 0.163 E_o^{0.757}} \quad (1.27)$$

1.3.2.4 Turbulent Dispersion Force

The turbulent dispersion force is computed following the General Turbulent Dispersion approach presented by Lavieille *et al.* [68]:

$$\overline{F_{V,TD}} = -\overline{F_{L,TD}} = -\frac{2}{3} \alpha_L \alpha_V C_{TD} \bar{\nabla}(\alpha_V) \quad (1.28)$$

The value of C_{TD} notably depends on the fluid turbulence, drag force, added mass force. Further details on its derivation are presented in Lavieille *et al.* [68].

1.4 TURBULENCE MODELING

For bubbly flow simulations, only liquid phase turbulence is taken into account while it is neglected for the vapor phase. The prescribed model is the Reynolds Stress Model $R_{ij} - \varepsilon$ SSG from Speziale, Sarkar and Gatski [111] adapted to two-phase boiling flows by Mimouni *et al.* [88]. Noting $R_{ij} = \langle U'_{L,i} U'_{L,j} \rangle_L$ and $\alpha = \alpha_V$, it reads:

$$(1 - \alpha) + \frac{D\rho_L R_{ij}}{Dt} = \frac{\partial}{\partial x_k} \left[\left(\rho_L \nu_L + \rho_L C_s \frac{k}{\varepsilon} R_{ij} \right) \frac{\partial}{\partial x_k} ((1 - \alpha) R_{ij}) \right] \quad (1.29)$$

$$+ (1 - \alpha) (P_{ij} + G_{ij} + \Phi_{ij} + \varepsilon_{ij}) \quad (1.30)$$

where D/Dt is the Lagrangian derivative, k the turbulent kinetic energy, ε the turbulent pseudo-dissipation rate, \bar{P} the turbulent production term, \bar{G} the gravity production, $\bar{\Phi}$ the pressure-strain term and $\bar{\varepsilon}$ the viscous destruction term.

All those terms need a proper modeling, for which we refer the reader to Mimouni *et al.* [88].

The transport equation on ε also includes the impact of α :

$$(1 - \alpha) + \frac{D\varepsilon}{Dt} = \frac{\partial}{\partial x_k} \left[C_\varepsilon \frac{k}{\varepsilon} \langle U'_{L,k} U'_{L,l} \rangle_L \frac{\partial (1 - \alpha) \varepsilon}{\partial x_l} \right] \quad (1.31)$$

$$+ \left(C_{\varepsilon_1} + C_{\varepsilon_3} G + C_{\varepsilon_4} k \frac{\partial U_{L,k}}{\partial x_k} - C_{\varepsilon_2} \varepsilon \right) \frac{(1 - \alpha) \varepsilon}{k} \quad (1.32)$$

We conclude by specifying the values used for the constants in NEPTUNE_CFD (Table 1.1).

C_s	C_1	C_2	C_1^ω	C_2^ω	C_ε	C_{ε_1}	C_{ε_2}	C_{ε_3}	C_{ε_4}
0.2	1.8	0.6	0.5	0.3	0.18	1.44	1.92	1.44	0.33

Table 1.1: Constant values for the SSG model in NEPTUNE_CFD

1.5 WALL BOILING MODEL

The modeling of the heterogeneous boiling phenomenon at the wall is based on a Heat Flux Partitioning (HFP) model, from Kurul & Podowski original work[66] who divided the wall heat flux density ϕ_w in three terms :

- A single phase convective heat flux $\phi_{c,L}$ heating the liquid through the fraction of the wall area unaffected by the vapor bubbles ;
- A vaporization heat flux ϕ_e which accounts for the generation of vapor through heterogeneous nucleation ;
- A quenching heat flux ϕ_q to represent the thermal impact of bubbles departing from the wall and being replaced by cool liquid

A fourth flux is added to this HFP in NEPTUNE_CFD, following Mimouni *et al.* [87] who consider a convective heat flux towards the vapour $\phi_{c,V}$ when the wall area is covered by a dense accumulation of bubbles.

The model is then ponderated by a phenomenological function f_{α_L} enhancing $\phi_{c,V}$ when the void fraction at the wall becomes large. It thus gives Equation 1.33 :

$$\phi_w = f_{\alpha_L} (\phi_{c,L} + \phi_e + \phi_q) + (1 + f_{\alpha_L}) \phi_{c,V} \quad (1.33)$$

where f_{α_L} verifies smooth conditions $\lim_{\alpha_L \rightarrow 1} f_{\alpha_L} = 1$, $\lim_{\alpha_L \rightarrow 0} f_{\alpha_L} = 0$, $\lim_{\alpha_L \rightarrow 0} \frac{f_{\alpha_L}}{\alpha_L} = 0$ and $\lim_{\alpha_L \rightarrow 1} \frac{1 - f_{\alpha_L}}{1 - \alpha_L} = 0$.

The convective heat fluxes are expressed as:

$$\phi_{c,k} = A_k h_{k,\log} (T_w - T_k) \quad (1.34)$$

$$h_{k,\log} = \frac{\rho_k c_{p,k} U_\tau}{T_L^+} \quad (1.35)$$

where A_k the fraction of the wall area facing phase k , T_w the wall temperature and $h_{k,\log}$ the wall logarithmic convective heat transfer coefficient to phase k based on the wall functions for friction velocity U_τ and non-dimensional liquid temperature T_L^+ described in 1.6.

The vaporization heat flux is computed following:

$$\phi_e = N_{sit} f \rho_V h_{LV} \frac{\pi D_d^2}{6} \quad (1.36)$$

Closure of physical parameters needed are :

- N_{sit} the nucleation site density modeled as [71]:

$$N_{sit} = [210 (T_w - T_{sat})]^{1.8} \quad (1.37)$$

- f the bubble detachment frequency expressed as [19]:

$$f = \sqrt{\frac{4}{3} \frac{g |\rho_V - \rho_L|}{\rho_L D_d}} \quad (1.38)$$

- D_d the bubble detachment diameter given by Ünal correlation [139] corrected by Borée *et al.* [7] (Equation 1.39).

$$D_d = 2.42 \times 10^{-5} P^{0.709} \frac{a}{\sqrt{b\varphi}} \text{ with} \quad (1.39)$$

$$a = \frac{(T_w - T_{sat}) \lambda_w}{2\rho_V h_{LV} \sqrt{\pi\eta_w}} \quad (1.40)$$

$$b = \begin{cases} \frac{T_{sat} - T_L}{2 \left(1 - \frac{\rho_V}{\rho_L} \right)}, & \text{if } St \leq 0.0065 \\ \frac{1}{2(1 - \rho_G/\rho_L)} \frac{\phi_{c,L} + \phi_e + \phi_q}{0.0065 \rho_L c_{p,L} \|\bar{U}_L\|}, & \text{if } St > 0.0065 \end{cases} \quad (1.41)$$

where λ_w and η_w are the wall thermal conductivity and diffusivity, $St = \frac{\phi_{c,L} + \phi_e + \phi_q}{\rho_L c_{p,L} \|\bar{U}_L\| (T_{sat} - T_L)}$ is the Stanton number and $\varphi = \max \left(1; \left(\frac{\|\bar{U}_L\|}{U_0} \right)^{0.47} \right)$ with $U_0 = 0.61 \text{ m/s}$

Finally, the quenching heat flux follows the approach of Del Valle & Kenning [24] supposing that it follows a semi-infinite transient conduction regime:

$$\phi_q = A_G t_q f \frac{2\lambda_L (T_w - T_L)}{\sqrt{\pi\eta_L t_q}} \quad (1.42)$$

where t_q is the quenching time, supposed to be equal to $1/f$.

1.6 WALL FUNCTION FOR DISPERSED BOILING FLOWS

In boiling flows, the formation of bubbles at the wall may disturb the liquid velocity profile in the boundary layer. To take this phenomena into account, Mimouni *et al.* [87] proposed a wall function for boiling flows which tends to the single-phase formulation when $\alpha_V \rightarrow 0$ and depends on the bubble diameter and density at the wall:

$$U^+ = \frac{1}{\kappa} \ln(y^+) + B - \Delta U^+ \text{ with} \quad (1.43)$$

where $\kappa=0.41$ is the Von Karman constant, $B = 5.3$ the standard single-phase logarithmic law constant and ΔU^+ represents the offset of U^+ due to the wall roughness induced by the presence of bubble.

The correction Δu^+ is computed as:

$$\Delta U^+ = \begin{cases} 0 & \text{if } k_r^+ \leq 11.3 \\ \frac{1}{\kappa} \ln(1 + C_{kr} k_r^+) & \text{if } k_r^+ > 11.3 \end{cases} \quad (1.44)$$

$$k_r^+ = \frac{k_r \sqrt{U_T U_T}}{\nu_L} \quad (1.45)$$

$$k_r = \alpha_V d_V \quad (1.46)$$

$$U_T = C_\mu^{1/4} \sqrt{k_L} \quad (1.47)$$

with $C_{kr} = 0.5$, k_r a "bubble roughness Reynolds number", $C_\mu = 0.09$ defined from the $k - \varepsilon$ and k_L the liquid turbulent kinetic energy.

The non-dimensional wall liquid temperature T_L^+ is modeled according following a Van Driest formulation:

$$T_L^+ = \int_0^{y^+} \frac{2dy}{1 + \frac{1}{2} \frac{\Pr_L}{\Pr_T} \sqrt{1 + 4\kappa^2 y^{+2} (1 - \exp(-y^+/A))^2}} \quad (1.48)$$

with $A = 25.6$, $\Pr_T = 0.9$ and $y^+ \approx 100$ usually.

2

FLOW BOILING EXPERIMENTS REPRESENTATIVE OF PWR: THE DEBORA DATABASE

Contents

2.1	Introduction	10
2.2	Simulating PWR water using R12	10
2.2.1	Conservation of the Phase Density Ratio	11
2.2.2	Conservation of the Weber Number	11
2.2.3	Conservation of the Boiling Number	12
2.2.4	Conservation of the Inlet Thermodynamic Quality	12
2.2.5	Same Geometry	13
2.2.6	Transposition ranges	13
2.3	Description of the Test Section	13
2.3.1	Geometrical Description	13
2.3.2	Measurement Instrumentation	14
2.4	Measurements Campaigns and Results	16
2.4.1	Cases Nomenclature and Test Series	16
2.4.2	Verification of Control Parameters Coherency	17
2.4.3	Qualitative Analysis of the Experimental Results	19
2.5	Further Verifications	23
2.5.1	Reconstruction of the Applied Heat Flux	23
2.5.2	Verification of Wall Temperature Measurements	26
2.6	Conclusions	28

2.1 INTRODUCTION

The validation of any existing modeling of multiphase flows must rely on extensive databases from experimental investigations in operating conditions that are representative of industrial configurations in PWR. This naturally lead to an important demand for measurements of local phase-related properties of vertical pressurized subcooled boiling flows.

To meet this need, CEA and EDF built a test facility called DEBORA in the 1990's. Its goal was to establish a consistent database of local measurements of the flow structure for vertical subcooled boiling freon Refrigerant 12 (R12) from the Onset of Nucleate Boiling to the Boiling Crisis.

Many authors contributed to the establishment and analysis of the DEBORA database, among which Cubizolles [22], Garnier *et al.* [35], Manon [79], Guéguen [44] or Klédy [60].

In this chapter, we will describe the test section and analyze the available results from past measurements campaigns.

2.2 SIMULATING PWR WATER USING R12

The choice of using R12 as the working fluid in the DEBORA loop emerged from the interesting properties that boiling freon presents when compared to the highly pressurized water in PWR cores. Indeed, the conditions for which the Boiling Crisis must be studied for water in PWR are:

- Pressure P between 100 and 180 bar ;
- Inlet liquid mass flux G between 1000 and 5000 kg/m²/s ;
- Wall heat flux ϕ_w between 0.5 and 6 MW/m² ;
- Inlet thermodynamic flow quality $x_{eq,in}$ between -0.4 and 0.4.

In those ranges, sensors dedicated to local measurements are not suited to sustain such conditions.

The experimental strategy is then to "simulate" the aimed industrial conditions using a different fluid. It has to present thermophysical properties that allow to reproduce non-dimensional numbers of the industrial flow using less constraining operating conditions.

This explains the choice of R12 as it permits to transpose relevant parameters for PWR as detailed below.

2.2.1 Conservation of the Phase Density Ratio

Freon 12 can reach the same density ratio as water in PWR using limited pressurized conditions no larger than 30 bars. It is an important parameter to mimic the behavior of the boiling two-phase flow since it has a strong influence over the bubble size for example [62].

$$\left(\frac{\rho_{V,sat}}{\rho_{L,sat}} \right)_{P_1}^{water} = \left(\frac{\rho_{V,sat}}{\rho_{L,sat}} \right)_{P_2}^{R12} \quad (2.1)$$

with $P_2 < P_1$.

The evolution of the density ratio of water and R12 with pressure are shown on Figure 2.1.

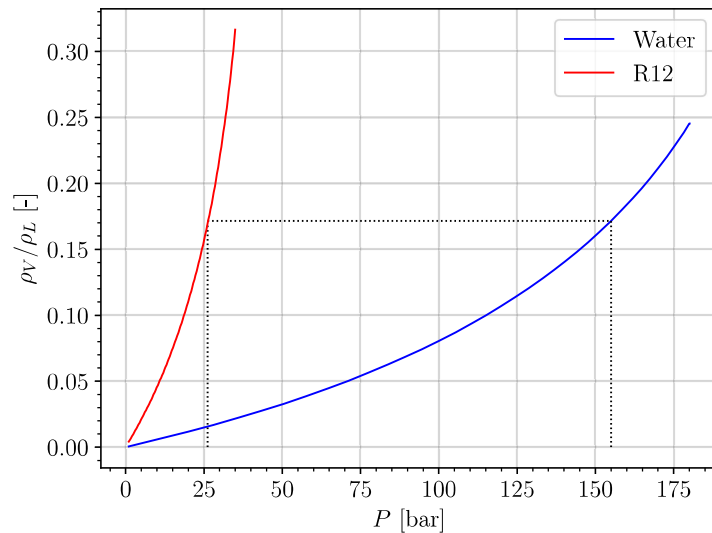


Figure 2.1: Density ratio of pressurized R12 and water

For instance, we can see that R12 at approximatively 26 bar ($T_{sat} \approx 86.8^\circ\text{C}$) has the same density ratio as water at 155 bar ($T_{sat} \approx 344.8^\circ\text{C}$).

Note : This tranposition criteria thus scales the operating pressure P of the experiment.

2.2.2 Conservation of the Weber Number

The Weber number is also similar to those encountered in PWR.

$$We = \frac{G^2 R}{\rho_L \sigma} \quad (2.2)$$

This number characterizes physical phenomena such as bubble break-up or deformation under the influence of the liquid inertia.

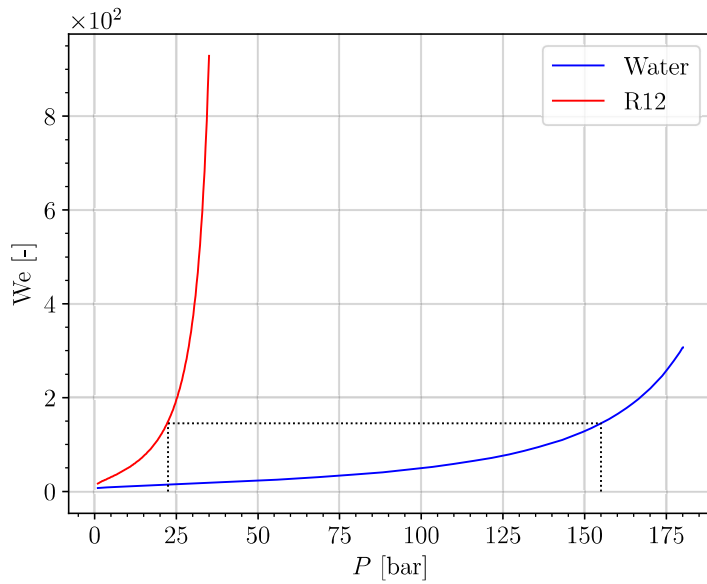


Figure 2.2: Weber number for R12 and water at $G = 2000 \text{ kg/m}^2/\text{s}$ and $R = 0.1 \text{ mm}$

Similar to the phase density ratio, Figure 2.2 shows that Weber number equivalent to water at 155 bar can be reached with R12 around 23 bar.

Note : For a same value of R , this transposition scales the inlet liquid mass flux G .

2.2.3 Conservation of the Boiling Number

The boiling number is defined as:

$$\text{Bo} = \frac{\phi_w}{G h_{LV}} \quad (2.3)$$

It represents the comparison between the vapor mass flux ϕ_w/h_{LV} if all the heat flux contributes to phase change versus the inlet liquid mass flux. Thus, its value can be associated to the boiling and two-phase flow regime.

Figure 2.3 shows that Boiling number values similar to PWR can be reproduced using R12 with wall heat fluxes one order of magnitude lower and pressure around 23 bar.

Note : This transposition criteria scales the applied heat flux ϕ_w .

2.2.4 Conservation of the Inlet Thermodynamic Quality

Water in PWR being highly subcooled to avoid boiling, reproducing the inlet subcooling in the DEBORA experiment allows to mimic the early stages of boiling between the ONB and OSV. It allows to reproduce Boiling Crisis by Departure from Nucleate Boiling for low quality flows. This is achieved through the inlet thermodynamic quality:

$$x_{eq,in} = \frac{h_{L,in} - h_{L,sat}}{h_{LV}} \quad (2.4)$$

Note : This transposition is achieved by scaling the R12 inlet temperature.

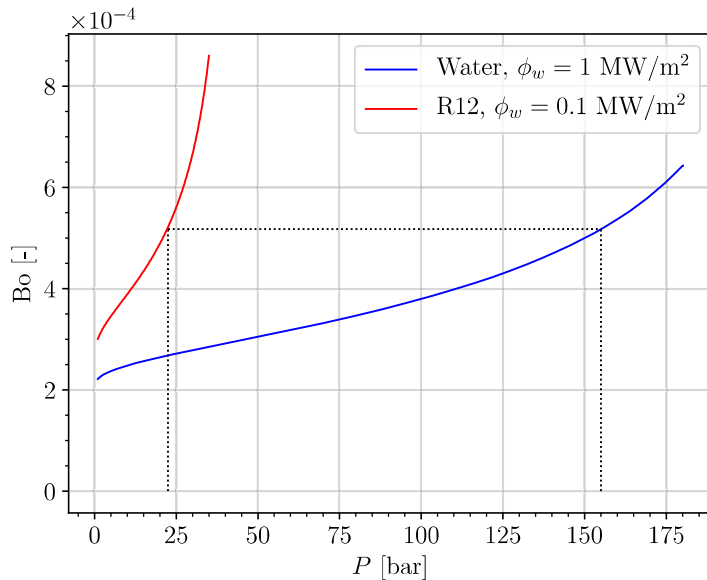


Figure 2.3: Boiling number for R12 and water at $G = 2000 \text{ kg/m}^2/\text{s}$

2.2.5 Same Geometry

The last similarity achieved in the DEBORA experiment is related to the geometry. The heated length L_{ch} of the test section is similar to the height of a nuclear fuel assembly and the hydraulic diameter D_h is equal to that of a subchannel.

2.2.6 Transposition ranges

As a result of those conservation criteria, Table 2.1 sums up the transposition ranges for each parameters.

Fluid	Water	Freon R12
P [bar]	100 - 180	14 - 30
G [$\text{kg}/\text{m}^2/\text{s}$]	1000 - 5000	1000 - 5000
ϕ_w [MW/m^2]	0.5 - 6	0.05 - 0.65
$x_{eq,in}$ [-]	(-0.4) - (+0.4)	(-0.4) - (+0.4)
$\rho_{V,sat}/\rho_{L,sat}$ [-]	0.08 - 0.25	0.07 - 0.22
We [-]	49.5 - 307.1	69.1 - 365.8
$Bo \times 10^{-3}$ [-]	0.19 - 3.86	0.21 - 4.33

Table 2.1: Water R12 scaling, $R = 0.01\text{mm}$ for We

2.3 DESCRIPTION OF THE TEST SECTION

2.3.1 Geometrical Description

To apply the aforementioned transport criteria, four thermal-hydraulic control parameters are imposed in the test section:

- The outlet pressure P ;
- The inlet mass flow rate $G \times S_{in}$ with $S_{in} = \pi R^2 \approx 2.9 \times 10^{-4} \text{ m}^2$ the inlet area ;
- The inlet liquid temperature $T_{L,in}$;
- The electrical power transferred to the liquid $\phi_w \times S_{heat}$ with S_{heat} the heated area.

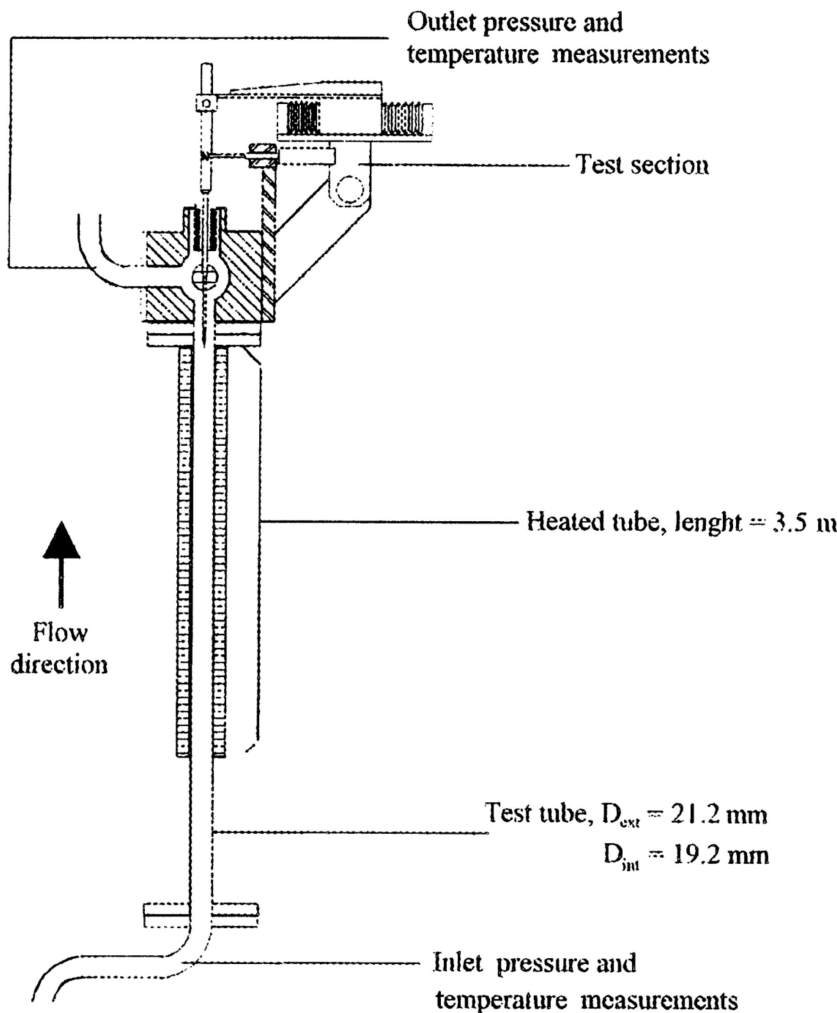


Figure 2.4: Sketch of the DEBORA test section. Adapted from [35].

The test section is presented on Figure 2.4. It consists of an inconel tube with inner diameter $D_h = 19.2$ mm, a 1 mm thickness and a heated length $L_{\text{heat}}=3.5$ m. A detailed description of the whole experimental loop is given in Garnier *et al.* [35].

2.3.2 Measurement Instrumentation

The control parameters are adjusted and measured using pressure, temperature, flow rate and power measurements. They are further detailed in Cubizolles [22].

The local measurements are conducted at the end of the heating length using a controllable probe that can cover the whole diameter of the test section with an accuracy of $10\mu\text{m}$. Only one diameter is covered since the chosen geometry induces an axisymmetry.

Three type of measurements have been conducted over different experimental campaigns.

2.3.2.1 Mono-Optical Probe Measurements

Optical probe measurement rely on the difference of optical refractive index between the liquid and vapor phase. Using an optical fiber in which light is emitted towards the probe tip allows to detect the actual phase flowing on the probe.

The resulting signal is called a Phase Indicator Function (PIF) which looks like to a square signal (Figure 2.5) that can be post-processed to identify the average time spent by the probe in each phase and then estimate their volume fraction *e.g.* the void fraction.

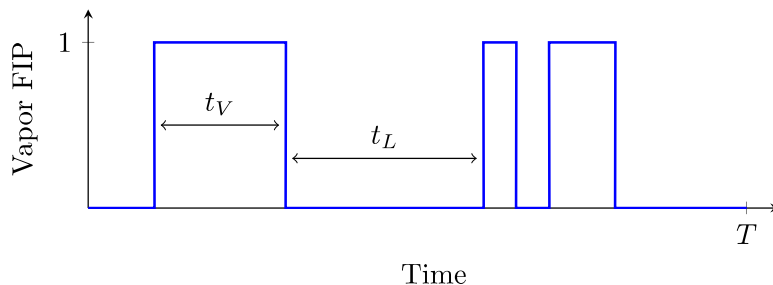


Figure 2.5: Example of Phase Indicator Function signal

If the PIF is measured over a period T , the void fraction α at the measurement point x can be estimated by:

$$\alpha(x) = \nu(x) \overline{t_V} = \frac{1}{T} \sum t_V \quad (2.5)$$

where ν is called the interference frequency that represents the number of phase interface detection per second by the probe.

Note : This measurement technique was performed in the **measurement campaign C2900** where void fraction profiles at the outlet were obtained for various flow conditions.

2.3.2.2 Bi-Optical Probe Measurements

Using the technology of the optical phase detection, adding a second optical probe permits to measure more parameters of the two-phase flow. Indeed, the use of two probes placed close to each other with a small shift in the flow direction (Figure 2.6) allows to estimate the velocity of the interface between the two probes by measuring the time difference between the two PIF.

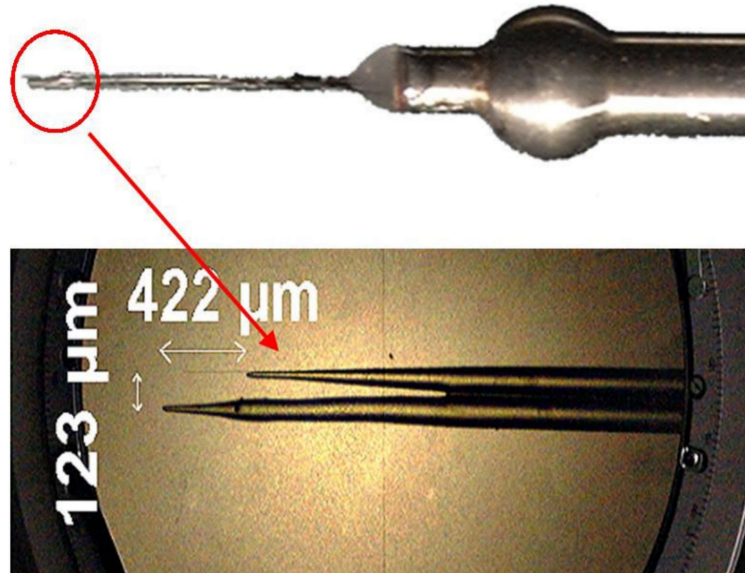


Figure 2.6: Picture of the bi-optical probe with a zoom over the two optical fibers. Reproduced from [44].

Considering the following assumptions:

- The flow is mainly one-directional in aligned with the probes ;
- The vapor phase is composed of spherical inclusions ;
- The velocity gradient and center density gradient are small along a bubble diameter length.

Then we can estimate:

- The vapor axial velocity $U_{V,z}$ that can be supposed equal to the measured interface velocity between the probes ;
- The interfacial area density a_i :

$$a_i = \frac{4\nu}{U_{V,z}} \quad (2.6)$$

- The bubble Sauter diameter:

$$D_V = \frac{6\alpha}{a_i} \quad (2.7)$$

Note : This measurement technique was performed in the **measurement campaign C3000**.

2.3.2.3 Thermocouples Measurements

Thermal measurements are conducted using chromel-alumel thermocouples. The liquid temperature is measured along the outlet diameter at the end of the heating length. Wall temperature measurements are conducted with 4 thermocouples placed at different heights (1.465 m, 2.465 m, 2.965 m, 3.485 m) on the outside of the tube.

Note : This measurement technique was performed in the **measurement campaign C800**.

2.3.2.4 Measurements Uncertainties

On Table 2.2 we mention the uncertainties associated to each control parameter and measurement.

Quantity	Notation	Uncertainty
Mass flux	G	$\pm 1\%$ (relative)
Outlet pressure	P	5000 Pa (absolute)
Inlet temperature	$T_{L,in}$	$\pm 0.2^\circ\text{C}$ (absolute)
Heat flux	ϕ_w	$\pm 4\%$ (relative)
Void fraction	α	$\pm 2\%$ (absolute)
Bubble diameter	D_V	$\pm 12\%$ (relative)
Vapor velocity	$U_{V,z}$	$\pm 10\%$ (relative)
Wall & liquid temperature	T_w & T_L	$\pm 0.2^\circ\text{C}$ (absolute)

Table 2.2: Uncertainties for DEBORA results [22, 44]

2.4 MEASUREMENTS CAMPAIGNS AND RESULTS

2.4.1 Cases Nomenclature and Test Series

As mentioned before, three different campaigns have been performed:

- Campaign C2900 with solely void fraction measurements using mono-optical probe ;
- Campaign C3000 with void fraction, vapor velocity, bubble Sauter diameter and interfacial area density measurements using bi-optical probe ;
- Campaign C800 with liquid and wall temperature measurements using thermocouples.

Each measurement series is conducted under fixed outlet pressure, liquid mass flux and electrical power. Inlet temperature is then changed to cover different inlet quality. Experimental cases are named in the form **CccGgPppWwwTett** with **cc** the campaign number (29, 30 or 8), **g** the inlet mass velocity (G in $\text{t/m}^2/\text{s}$), **pp** the outlet pressure (P in bars), **ww** the total heat power applied (Φ_w in kW) and **tt** the inlet temperature ($T_{L,in}$ in K). For instance, the case named C30G2P26W16Te66 has been conducted with $P = 26.2$ bar, $G = 2049 \text{ kg/m}^2/\text{s}$, $\Phi_w = 15.6 \text{ kW} \equiv \phi_w = 73.89 \text{ kW/m}^2$ and $T_{L,in} = 66.59^\circ\text{C}$.

P	G	W16	W17	W23	W24	W25	W27	W29	W30	W31	W33	W34	W36	W38	W39	W40	W42	W44
14	2	○	▽	△														
	4				○				▽	▽		▽	▽	▽	▽	▽	▽	▽
	5																	
26	2	○	▽	△			▽	△	▽	▽	△	▽	△	▽	▽	△	▽	△
	3			▽	△	○	▽	△	▽	▽	△	▽	△	▽	▽	△	▽	△
	5	○																

P	G	W12	W14
30	1	▽	▽

Table 2.3: Test matrix of the DEBORA cases. ○: C800 - ▽: C2900 - △: C3000

If we want to obtain a full description of the two-phase flow from the DEBORA tests, we need to have measurements from campaigns C3000 and C800 (flow topology and thermal) with the same control parameters. Table 2.3 unfortunately shows that only very few test series between C3000 and C800 have common operating conditions, namely:

- Series 8G2P14W16 and 30G2P14W16 ;
- Series 8G2P26W16 and 30G2P26W16.

Other flow conditions have either been covered with thermal measurements or topology measurements but not both.

Remark : Cases from the campaign C2900 would only be relevant for void fraction profiles comparison. Estimations of the bubble diameter can not be achieved except if one assumes a velocity profile as suggested by Cubizolles [22] and re-used by Guéguen [44] who supposes:

$$U_{V,z}(r) \approx U_{M,z}(r) = 1.22 \frac{G}{\langle \rho_M \rangle_2} \left(\frac{R-r}{R} \right)^{1/7} \quad (2.8)$$

where $U_{M,z}$ is the mixture axial velocity, assuming a mechanical equilibrium between the phases.

For further studies, we will mainly focus on the G2P26W16 and G2P14W16 test series. Although we will mainly rely on the results from the C3000 campaign (where vapor velocity was actually measured) for flow topology qualification, we will evaluate the assumption of Eq. 2.8 with the C2900 measurements.

2.4.2 Verification of Control Parameters Coherency

For each case, the total heat input Φ_w is given along with the inlet mass flux G , inlet liquid temperature $T_{L,in}$ and outlet quality $x_{eq,out}$. To verify the consistency of those values, we can recalculate the outlet quality:

$$x_{eq,out,calc} = \frac{h_{M,out,calc} - h_{L,sat}}{h_{LV}} \quad (2.9)$$

with $h_{M,out,calc}$ the recalculated outlet mixture enthalpy:

$$h_{M,out,calc} = h_{in} + \frac{\Phi_w}{GS_{in}} = h_{in} + \frac{4\phi_w L_{heat}}{GD_h} \quad (2.10)$$

with h_{in} the inlet enthalpy calculated from the fluid properties using the inlet liquid temperature.

The difference between the given and recalculated outlet quality can also be converted to input power error by recalculating the heat needed to reach the given $x_{eq,out}$:

$$\Phi_{w,calc} = \frac{G\pi R^2}{\underbrace{[x_{eq,out}h_{LV} + h_{L,sat}] - h_{L,in}}_{h_{M,out}}} \quad (2.11)$$

Moreover, for a given set of experiments at the same P , G and Φ_w changing the inlet quality can be associated to moving the measurement diameter along the axial direction following the relationship:

$$x_{eq}(z) = x_{eq,in} + \frac{4\phi_w z}{GD_h h_{LV}} \quad (2.12)$$

Thus, taking the maximum inlet quality case $x_{eq,in,max}$ as a reference ($z = 3.5$ m), we can estimate the corresponding measurement height z_{eq} of each other cases if the inlet quality was $x_{eq,in,max}$.

We calculated the equivalent heights and outlet quality / power input errors for two series of the C3000 campaigns. Results are displayed on Tables 2.4 and 2.5.

$T_{L,in}$ [K]	$x_{eq,in,calc}$ [-]	$x_{eq,out,calc}$ [-]	$x_{eq,out}$ [-]	z_{eq} [m]	$x_{eq,out}$ error [-]	Φ_w error [kW]
22.39	-0.317	-0.0821	-0.0832	1.075	0.114 %	-0.078
26.8	-0.28	-0.0422	-0.0431	1.653	0.089 %	-0.061
28.76	-0.263	-0.0267	-0.0273	1.896	0.056 %	-0.038
30.08	-0.252	-0.0152	-0.0157	2.065	0.05 %	-0.034
31.39	-0.241	-0.004	-0.0043	2.234	0.035 %	-0.023
38.95	-0.175	0.0674	0.0681	3.229	-0.072 %	0.049
39.96	-0.166	0.077	0.0776	3.357	-0.063 %	0.042
41.16	-0.155	0.0875	0.0882	3.509	-0.064 %	0.043

Table 2.4: Recalculated control parameters for the 30G2P14W16 cases. ($T_{sat} = 58.07^\circ\text{C}$)

$T_{L,in}$ [K]	$x_{eq,in,calc}$ [-]	$x_{eq,out,calc}$ [-]	$x_{eq,out}$ [-]	z_{eq} [m]	$x_{eq,out}$ error [-]	Φ_w error [kW]
58.57	-0.395	-0.0893	-0.0819	1.792	-0.747 %	0.381
60.54	-0.370	-0.0650	-0.0578	2.072	-0.722 %	0.369
62.54	-0.344	-0.0392	-0.0318	2.369	-0.741 %	0.378
64.6	-0.318	-0.0123	-0.0050	2.674	-0.736 %	0.376
66.59	-0.292	0.0140	0.0213	2.973	-0.728 %	0.371
68.57	-0.266	0.0402	0.0473	3.271	-0.716 %	0.365
70.59	-0.239	0.0670	0.0743	3.583	-0.723 %	0.369

Table 2.5: Recalculated control parameters for the 30G2P26W16 cases. ($T_{sat} = 86.81^\circ\text{C}$)

As we can see, the given values of outlet quality for the 30G2P14W16 tests are coherent with the one-dimensional enthalpy balance with errors mostly less than 0.1% on the recalculated quality and less than 100 W on the recalculated power input. This naturally leads to an equivalent height very close to 3.5 m for the hottest case.

However, a more significant error is observed on the 30G2P26W16 cases where errors up to 0.75% on the outlet quality and close to 0.4 kW on the power input are found. Those values are significant especially

for cases close to saturation where uncondensed vapor will start to appear in the bulk. Moreover, this results in an equivalent height 8.3 cm longer than the actually 3.5m heated length.

Since the inlet temperature, mass flux and power input are controlled parameters for each test, it is likely that the error may come from the given value of outlet quality $x_{eq,out}$ which is calculated and not imposed.

Note : Similar quality / input power errors were obtained on corresponding C29 and C8 campaigns:

- Negligible errors on for 29G2P14W16 and 8G2P14W16 cases ;
- Roughly 0.7 % outlet quality error and 0.3 to 0.4 kW power error for 29G2P26W16 and 8G2P26W16 cases.

2.4.3 Qualitative Analysis of the Experimental Results

On Figures 2.7, 2.8, 2.9 and 2.10 we respectively plot the experimental measurements of cases 29/30G2P26W16, 8G2P26W16, 29/30G2P14W16 and 8G2P14W16. The colorbar representing the oulet quality of each test is based on the computed value of $x_{eq,out}$ (Eq. 2.9).

2.4.3.1 G2P26W16 cases

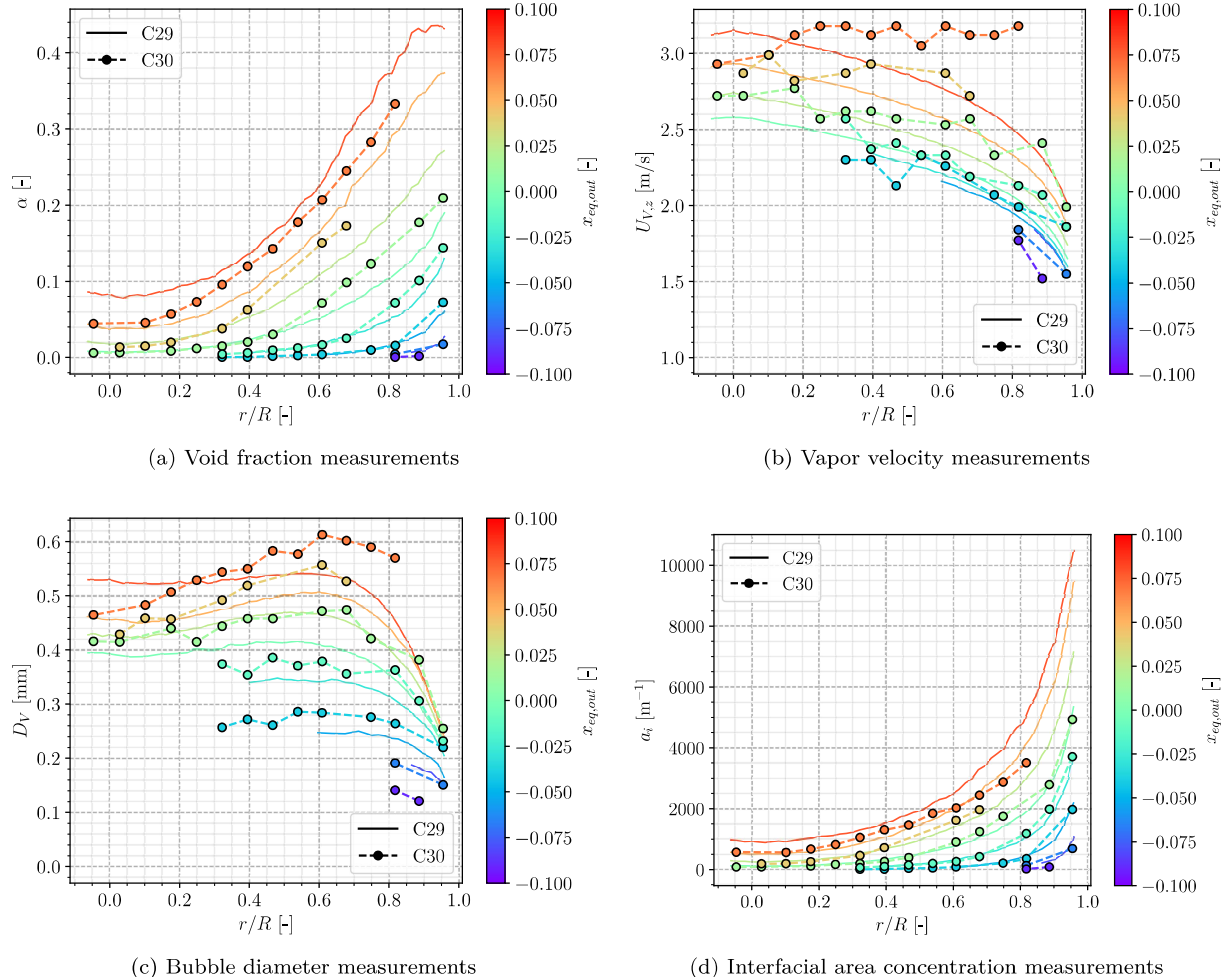


Figure 2.7: 30G2P26W16 and 29G2P26W16 results

Void fraction profiles obtained in for C2900 (single optical probe) and C3000 (bi-optical probe) cases are compared to verify the consistency of the measurements (Figure 2.7a). The two campaigns are in good

agreement with each other, displaying a void fraction profile monotonously increasing with the outlet quality. The estimation of the vapor velocity by Eq. 2.8 for the C29 results is acceptable but presents an growing underestimation as the outlet title increases (Figure 2.7b). This results in bubble diameter underestimation close to the wall and consequently interfacial area overestimation.

We observe that the void fraction naturally increases with the outlet quality and that we reach net vapor generation with $\alpha(R=0) > 0$ when $x_{eq,out} > 0$. Otherwise, vapor is not detected over the whole measurement section. Each case has its maximum void fraction near the wall with values up to approximately 40% when the outlet quality approaches 0.1.

The bubble diameter displays different behaviors (Figure 2.7c):

- It grows from the wall and reaches a maximum around $r/R \approx 0.6$, indicating bubble coalescence ;
- It stays nearly constant for negative outlet quality cases ;
- It decreases from $r/R = 0.6$ to $r/R = 0$ for saturated cases , indicating either bubble break-up or bulk condensation.

Remark : It seems that bubble diameter very close to the wall do not vary much between different cases, indicating that bubbles leave the wall at a nearly constant diameter over the different explored liquid temperatures ($D_V \approx 0.2$ mm).

Vapor velocity also increases with the outlet quality, with a nearly flat profile reached for saturated cases. The increase in vapor velocity may result of the larger bubble diameters which enhance the effect of buoyancy, acting as an accelerating term increasing the drift velocity.

Remark : Eq. 2.8 fails to predict this flattening of the vapor velocity on C2900 cases, which may indicate a change in the flow structure that can not be detected when assuming liquid-vapor mechanical equilibrium.

Regarding the liquid temperature measurements (Figures 2.8a and 2.8b), we see that temperature profiles linearly rise with the inlet quality while presenting an unmodified parabolic shape. The only change appears when reaching significant superheated conditions ($x_{eq,out} \sim 0.1$) where the liquid temperature profile flattens over the test section.

Moreover, we observe that measurements very close to the wall present a very large temperature gradient even for low quality cases (temperature jump of nearly 30 degrees for coldest cases). This jump reduces as flow quality increases and reduces even more for boiling cases, indicating the well-known rise of the global heat transfer coefficient in boiling regime vs. single-phase convection regime.

We can also note that for the hottest case, the liquid becomes superheated near the wall ($\Delta T_L(\pm 1) \approx 0.1^\circ\text{C}$). The bulk is still slightly subcooled with $\Delta T_L(0) = -1^\circ\text{C}$

Remark : The liquid being subcooled in the bulk for superheated cases hints that the decrease in bubble diameter observed in Figure 2.7c for $r/R < 0.6$ may be associated to condensation.

Wall temperature measurements (Figures 2.8c) display linear growth for subcooled cases which is in agreement with traditional liquid convection problems. When reaching boiling, the wall superheat stabilizes at $\Delta T_w \approx 2^\circ\text{C}$. Rearranging the different wall temperature measurements versus the local flow quality (Figure 2.8d) presents a coherent overlapping between cases with different inlet subcooling. This further validates the transposition of inlet quality into variation into an evolution of the measurement probe's axial position.

2.4.3.2 G2P14W16 cases

Similar to the G2P26W16 cases, we observe the consistency of the void fraction measurements between the C2900 and C300 campaigns (Figure 2.9a). Although the vapor velocity estimation using Eq. 2.8 for

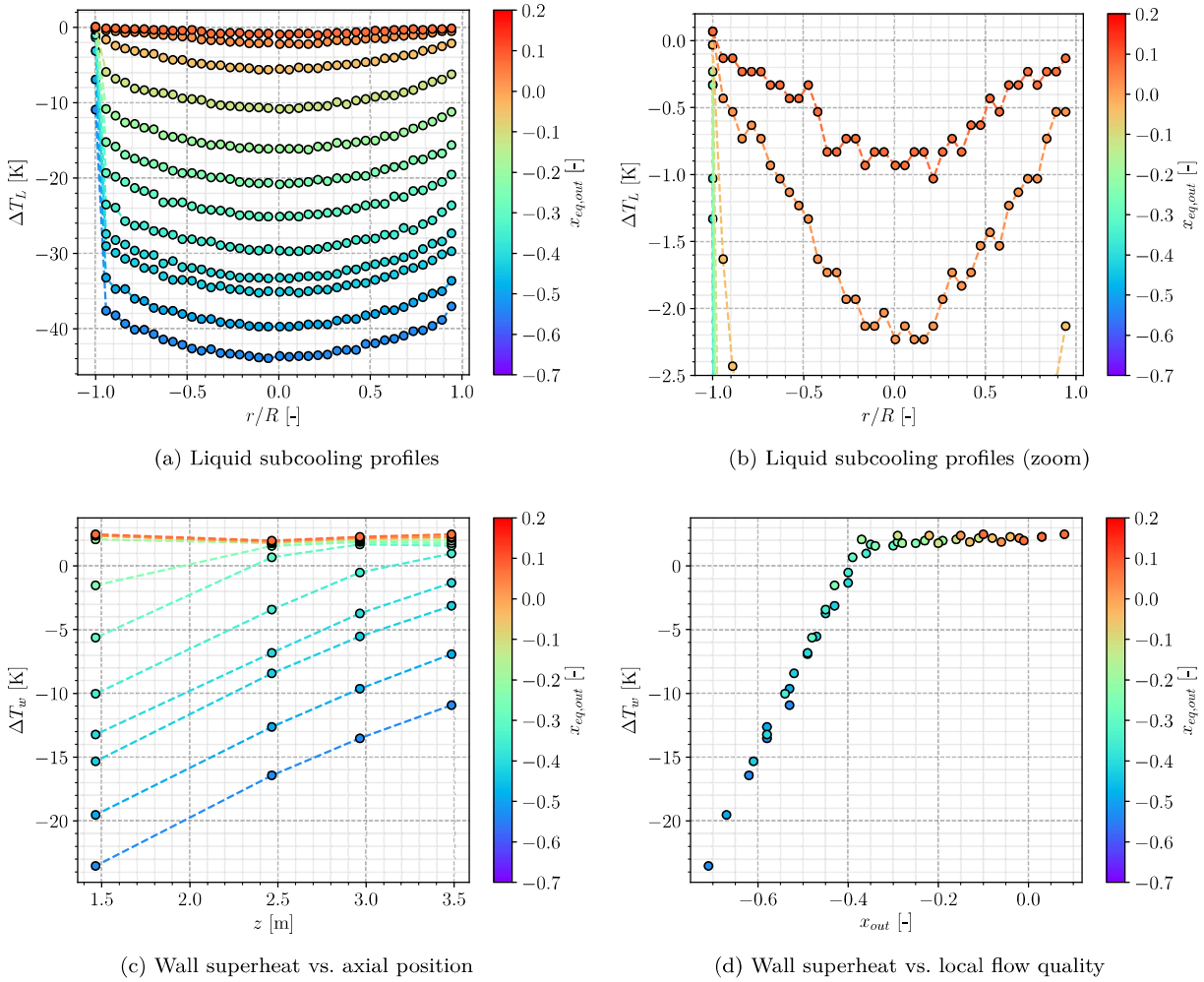


Figure 2.8: 8G2P26W16 results

C2900 cases also produces acceptable results for subcooled cases, the discrepancy when saturation is reached is even more observed here (Figure 2.9b). The overestimation when $x_{eq,out} > 0$ is larger than for the G2P26W16 cases, with nearly 1 m/s error on hottest cases.

This logically yields larger underestimations of the bubble diameter and associated overestimations of the interfacial area concentration.

The void fraction profiles (Figure 2.9a) present a particular evolution with a moving α peak that shifts from the wall to the bulk as the outlet quality increases. This may indicate a particular bubble dynamics regime inducing transverse bubble migration and accumulation far from the wall. Bulk void fraction can reach values as high as 70% with a flattening profile when $x_{eq,out} \rightarrow 0.1$.

Remark : It seems that saturated cases tend to reach a fixed value of near-wall void fraction between 35% and 40%.

Similar to previous observations, the bubble diameter grows when moving to the bulk, also presenting a peak value around $0.8 > r/R > 0.6$ for subcooled cases (Figure 2.9c). The saturated cases however present much larger increase in bubble diameter when reaching the bulk flow, with D_V close to 2 mm for the hottest case. This definitely indicates predominant coalescence effects.

Remark : $D_V \approx 2$ mm is observed at a point where $\alpha > 60\%$ which shows that even at such high void fraction values, the flow is still in a bubbly regime with small vapor inclusions ($D_V \approx 0.1D_h$).

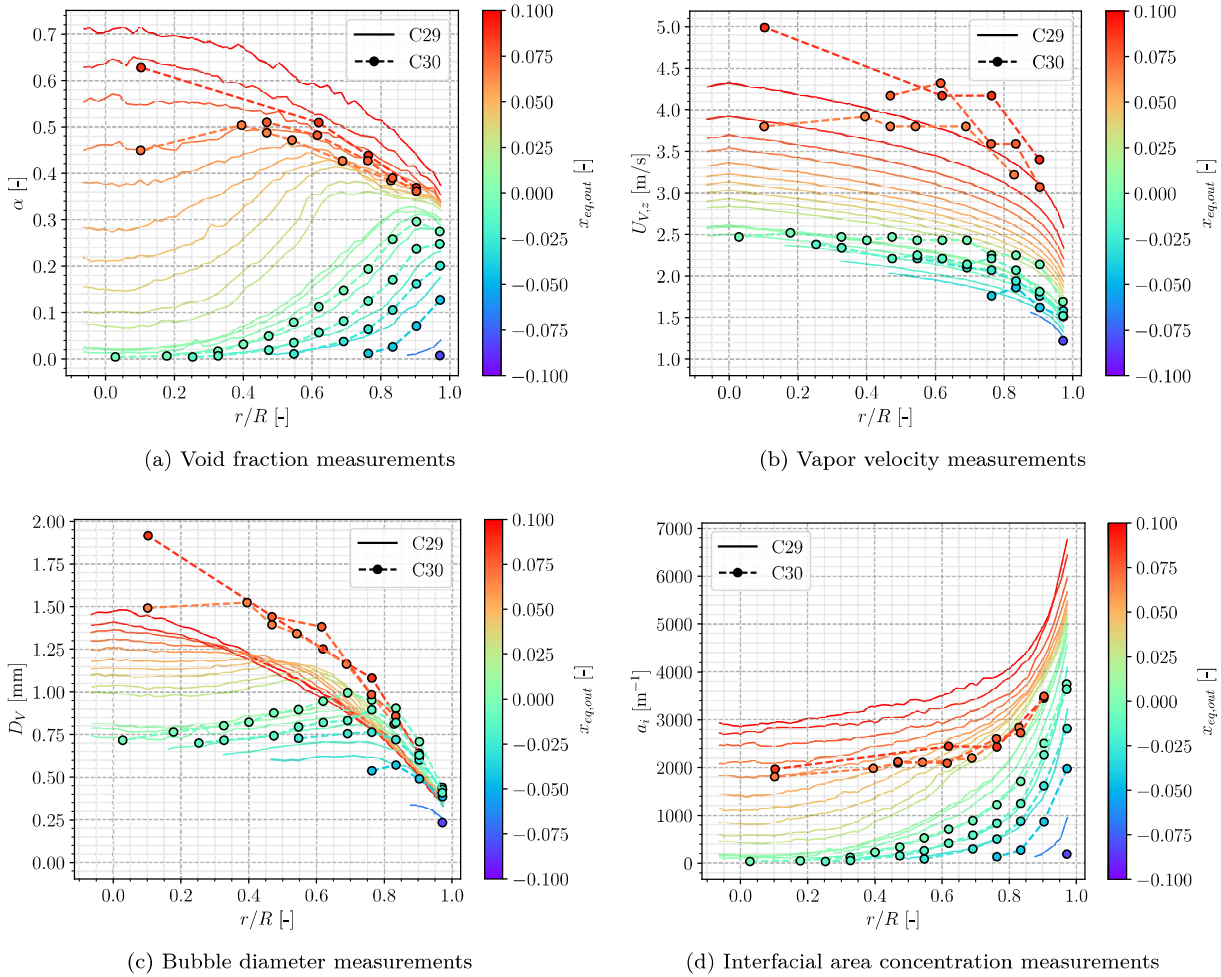


Figure 2.9: 30G2P14W16 and 29G2P14W16 results

The vapor velocity also increases with the outlet quality (Figure 2.9b), but reaches much larger value compared to the G2P26W16 cases. This may be due to the larger bubble size and local void fractions associated to the imposed mass flow rate.

The liquid temperature profiles (Figure 2.10a) are behaving in a very similar way to the G2P26W16 cases (Figure 2.8a): stable parabolic profile, linear shift with inlet quality and flattening when reaching superheated conditions ($x_{eq,out} \sim 0.1$).

We also have the huge temperature jump when approaching the wall which reduces when reaching boiling regimes. The measurements also detect superheated liquid near the wall for the hottest cases ($\Delta T_L \approx 0.1^\circ$). The case with the greatest outlet quality presents a surprisingly flat liquid temperature profile with measurements being nearly constant ($\Delta T_L = -0.3^\circ\text{C}$) over the whole measurement section.

Remark : Such a constant temperature profile could be interpreted as a limit of the liquid temperature in this regime. Since it corresponds to flow conditions where void fraction is large ($\alpha > 60\%$) and bubbles do not condense (Figure 2.9c), any extra heat input may only contribute to phase change and leave the liquid phase thermally unchanged.

Unfortunately, the 8G2P15W16 campaign did not cover as large quality range as the 8G2P26W16 campaign. We thus do not have access to many single-phase flow wall temperature measurements (Figure 2.10c). Only one point for $x_{eq,out} \approx -0.1$ seem to be in the single-phase convection region. All the other measurements are close to each other and correspond to boiling regimes where we observe a wall superheat stabilization around $\Delta T_w = 4^\circ\text{C}$.

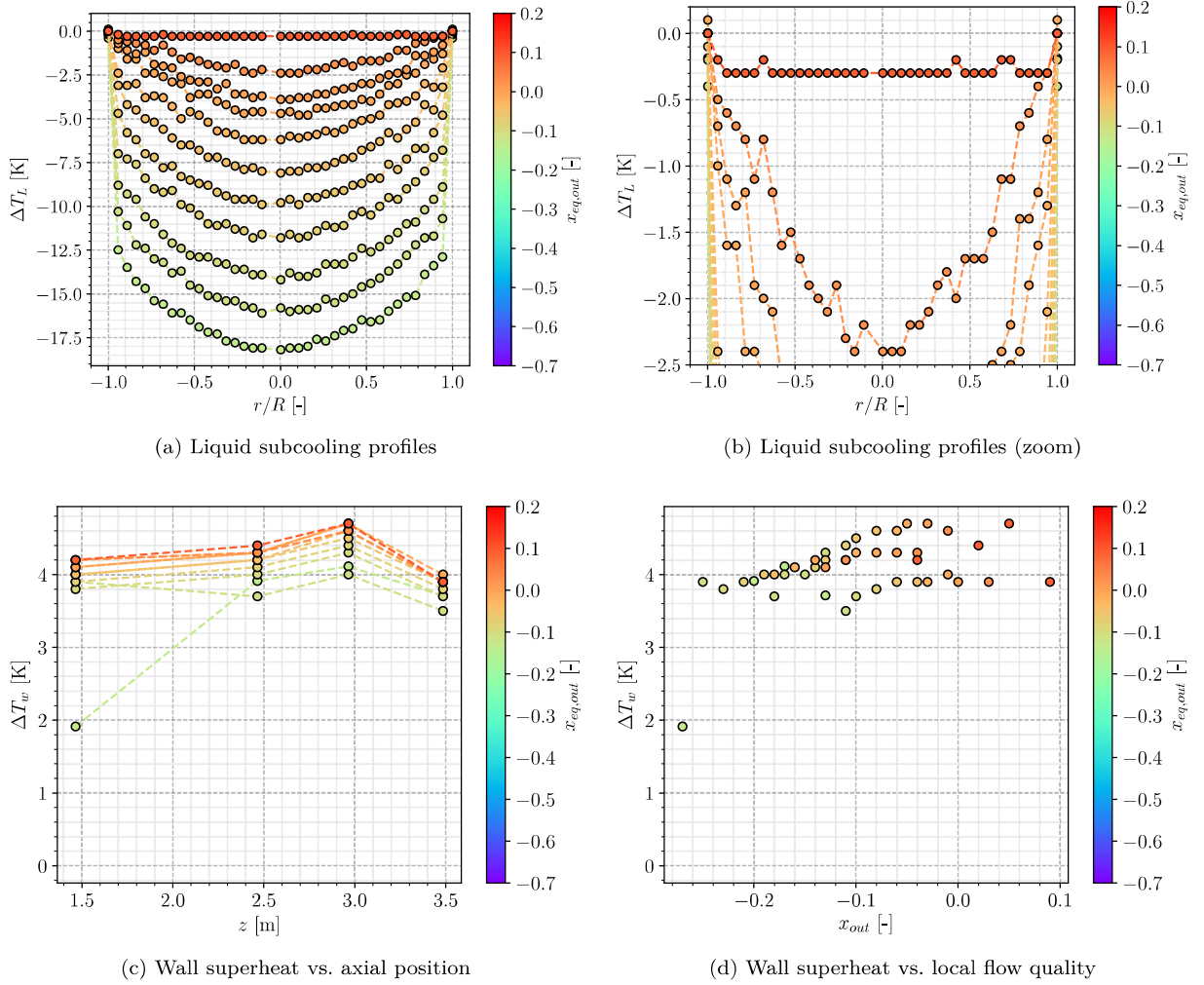


Figure 2.10: 8G2P14W16 results

The comparison of wall temperature with local flow quality (Figure 2.10d) is not as interesting as the G2P26W16 cases but still display a welcomed overlapping of the measurements over the different inlet temperatures.

2.5 FURTHER VERIFICATIONS

2.5.1 Reconstruction of the Applied Heat Flux

To further quantify the coherency of the DEBORA database, we want to reconstruct the wall heat flux injected in the flow from the experimental measurements of void fraction, vapor velocity and liquid temperature measurements.

2.5.1.1 Methodology

To do so, we will estimate the total enthalpy change between the inlet and outlet. The inlet liquid enthalpy $h_{L,in}$ is estimated using the inlet temperature and the outlet mixture enthalpy $h_{M,out}$ is computed as:

$$h_{M,out} = x_{m,out} h_{V,sat} + (1 - x_{m,out}) \langle h_{L,out} \rangle_2 \quad (2.13)$$

supposing that the vapor is at saturation temperature and where $x_{m,out}$ is the outlet mass quality.

Using the experimental values of α and $U_{V,z}$, we can compute the outlet mass quality $x_{m,out}$ as:

$$x_{m,out} = \frac{\rho_V \langle \alpha U_{V,z} \rangle_2}{G} \quad (2.14)$$

where:

$$\langle \alpha U_{V,z} \rangle_2 = \frac{1}{\pi R^2} \int_{\vartheta=0}^{2\pi} \int_{r=0}^R \alpha(r) U_{V,z}(r) r dr d\vartheta = \frac{2}{R^2} \int_{r=0}^R \alpha(r) U_{V,z}(r) r dr \quad (2.15)$$

for an axisymmetric profile such as the DEBORA measurements.

From the mass quality we can compute the mixture enthalpy as:

$$h_M = x_m h_{V,sat} + (1 - x_m) \frac{\langle \rho_L (1 - \alpha) U_{L,z} h_L \rangle_2}{\langle \rho_L (1 - \alpha) U_{L,z} \rangle_2} \quad (2.16)$$

Similarly, the average liquid enthalpy at the outlet is estimated as:

$$\langle h_L \rangle_2 = \frac{2}{R^2} \frac{1}{G_L} \int_{r=0}^R \rho_L(r) U_{L,z}(r) h_L(r) r dr \quad (2.17)$$

where h_L is estimated using the local temperature measurements and $U_{L,z}$ is estimated using the drift velocity of Ishii [51]:

$$U_{L,z} = U_{V,z} - U_{rel} = U_{V,z} - \sqrt{2} \left(\frac{g \sigma (\rho_L - \rho_V)}{\rho_L^2} \right)^{1/4} (1 - \langle \alpha \rangle_2)^{1.75} \quad (2.18)$$

Then, writing the one-dimensional energy balance of the flow permits to express the actually applied heat flux:

$$G \pi R^2 (h_{M,out} - h_{L,in}) = \Phi_w = \phi_w 2 \pi R L_{heat} \Rightarrow \phi_w = \frac{(h_{M,out} - h_{L,in}) G R}{2 L_{heat}} \quad (2.19)$$

which can be compared to the given control parameter for the experiment.

2.5.1.2 Application

To apply the presented reconstruction of the heat flux, we either need:

- A pure single-phase case with an outlet liquid temeprature profile (C800 case alone);
- A boiling two-phase case with void fraction and vapor velocity measurements (C3000 case) along with liquid temperature (C800 case).

This means that for boiling cases, we need to "merge" cases from the C3000 and C800 campaign conducted in very close operating conditions (P , G , $T_{L,in}$) and assume that the liquid temperature measurements of the C800 case are actually representative of the liquid temperature in the C3000 case and reciprocally for the void fraction and vapor velocity.

Such a constraint leaves us with very few boiling cases that can accommodate those conditions. They are summed up on Table 2.6.

Case Name	P [bar]	G [kg/m ² /s]	ϕ_w [kW/m ²]	$T_{L,in}$ [°C]	$x_{eq,in}$ [-]	$x_{eq,out}$ [-]
30G2P26W16Te66	26.2	2049.0	73.893	66.59	-0.2919	0.014
8G2P26W16Te66.6	26.2	1982.0	73.9	66.57	-0.2927	0.0237
30G2P26W16Te70	26.19	2051.2	73.893	70.59	-0.2386	0.067
8G2P26W16Te70.3	26.2	1983.0	73.9	70.31	-0.2428	0.0734

Table 2.6: Similar conditions cases between the C3000 and C800 campaigns. Outlet quality calculated with Eq. 2.9.

To actually compute the surface-averaged quantities, we need to interpolate the experimental profiles which is done using the python package `scipy`. Figure 2.11 presents typical interpolation profiles used in this sections.

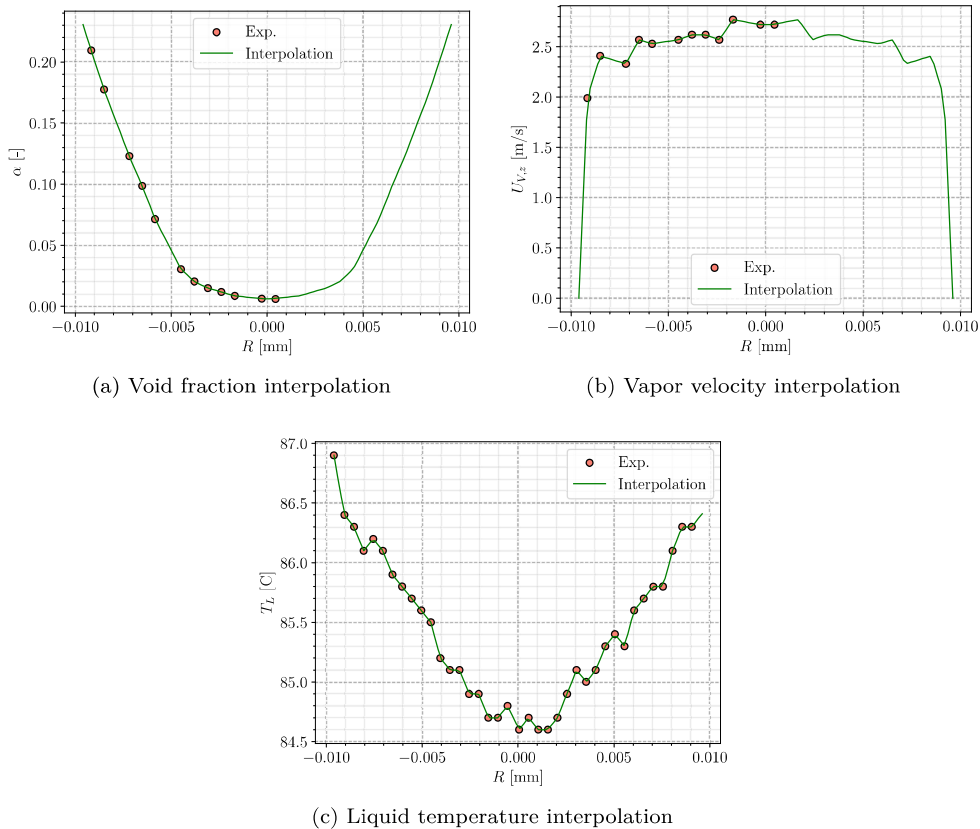


Figure 2.11: Interpolation profiles for cases Te66 (Table 2.6).

Case name	x_m [-]	$\phi_{w,rec}$ [kW/m ²]	$\phi_{w,exp}$ [kW/m ²]	$\Delta\phi_w$ [%]
30G2P26W23Te66	0.0193	70.432	73.893	-4.68%
30G2P26W23Te70	0.0500%	68.041	73.893	-7.9%

Table 2.7: Heat flux recalculation results

The results obtained for the heat flux recalculations are presented on Table 2.7.

We see that reconstructing the heat flux yields values significantly lower than the experimental values given in the database. The initial uncertainty of the wall heat flux being of 4% (Table 2.2), which is smaller than the computed values but close for the Te66 case.

This underestimation was also noted for single-phase C800 cases in a similar approach conducted by Guéguen [44] who found discrepancy up to 6%.

In our case, these discrepancies can be partially explained by:

- The difference of inlet mass fluxes that are roughly 70 kg/m²/s lower for the C800 cases ;
- The difference of inlet liquid temperature for the Te70 cases with a C800 case 0.3°C lower than the C300 case.

Those small discrepancies lead to outlet qualities (computed with Eq. 2.9 using the given ϕ_w) that differ of approximately 1%. Even though boiling flows near saturation, such as those studied here, are very sensitive to the local quality and flow parameters, this would hardly suffice to explain differences in heat flux as much as 5%.

Remark : Unfortunately, our methodology do not rely on collocated measurements of all the variables of interest since the campaigns were conducted separately. The "correction" values presented in Table 2.7 can not be considered as accurate estimations but still point out that an uncertainty over the heat flux can be considered in further work.

2.5.2 Verification of Wall Temperature Measurements

In order to test the coherency of wall temperature measurements both in single phase and boiling regions, we compare them to one-dimensional correlations along the $(\Delta T_w, x_{eq})$ curve.

Single-phase measurements are confronted to the estimations of Dittus–Boelter (Eq. 2.20, *DB*) correlation and Gnielinski correlation (Eq. 2.21, *G*):

$$\text{Nu}_{DB} = 0.023 \left(\text{Re}^{4/5} \right) \text{Pr}^{0.4} \quad (2.20)$$

$$\text{Nu}_G = \frac{\frac{C_f}{2} (\text{Re} - 1000) \text{Pr}}{1 + 12.7 \sqrt{\frac{C_f}{2}} (\text{Pr}^{2/3} - 1)} \quad (2.21)$$

where the friction coefficient C_f is estimated following Churchill [18] as recommended by Delhaye [25] and Guéguen [44]:

$$C_f = 2 \left[\left(\frac{8}{\text{Re}} \right)^{12} + \frac{1}{(A + B)^{1.5}} \right]^{1/12} \quad (2.22)$$

$$A = \left[2.457 \ln \left(\frac{1}{\left(\frac{7}{\text{Re}} \right)^{0.9} + 0.27 \frac{\varepsilon}{D_h} } \right) \right]^{16} \quad (\varepsilon=0 \text{ supposed here})$$

$$B = \left(\frac{37530}{\text{Re}} \right)^{16}$$

Wall superheat in boiling region is compared with the simple correlation of Frost & Dzakowic [33]:

$$\Delta T_{w,FD} = \text{Pr}_{L,sat} \sqrt{\frac{8\sigma\phi_w T_{sat}}{\lambda_{L,sat} h_{LV} \rho_V}} \quad (2.23)$$

where T_{sat} is expressed in Kelvin.

The results are presented on Figure 2.13 for cases at 26 bar and Figure 2.12 for cases at 14 bar. Since we do not need combination with void fraction measurements, every cases of the C800 campaign were used for comparison.

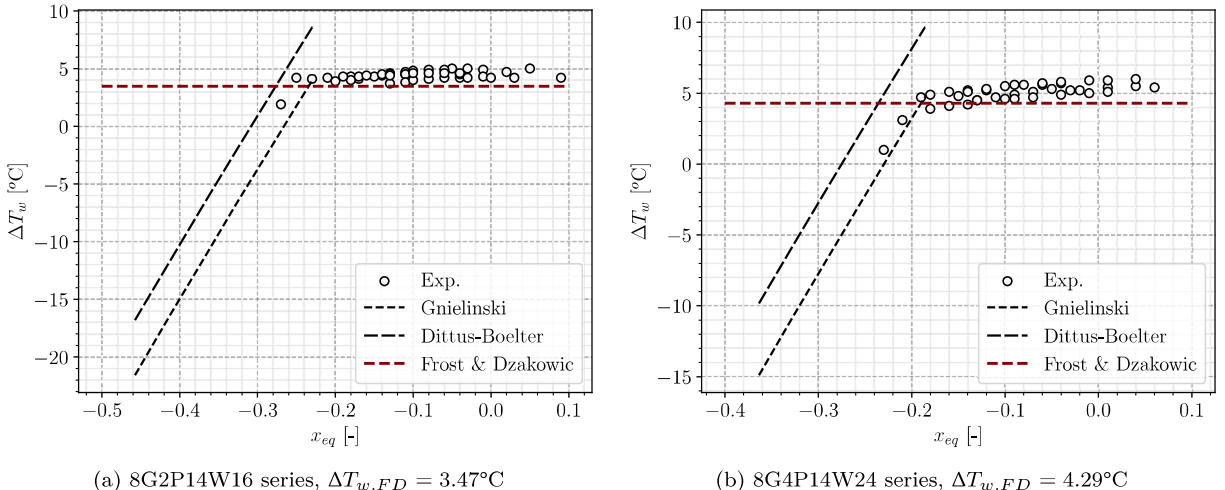


Figure 2.12: Correlations comparison with P14 cases.

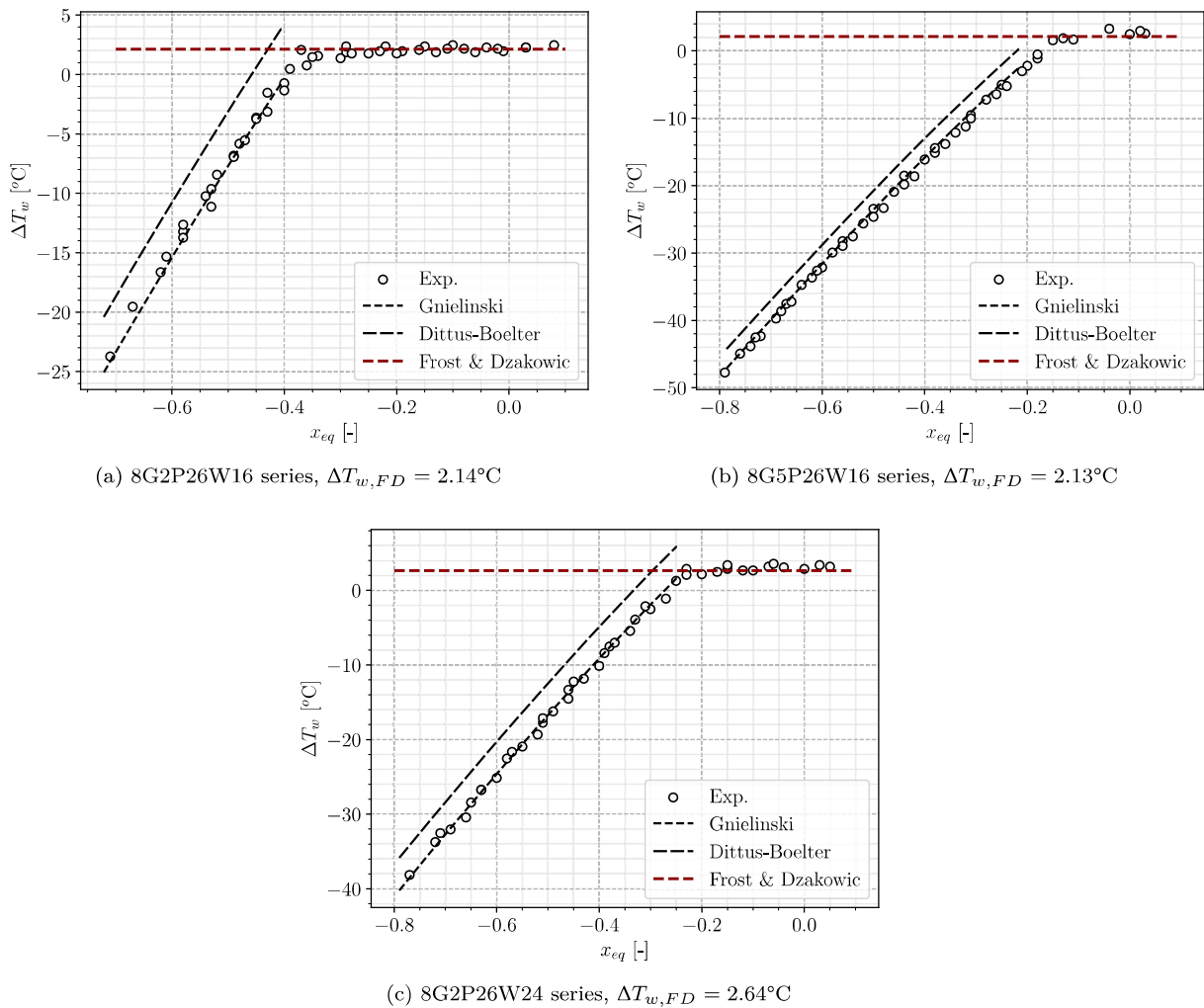


Figure 2.13: Correlations comparison with P26 cases.

Wall temperature measurements for the liquid convective regime are in fairly good agreement with the predictions of the Gnielinski correlation. The slope of the model is very close to the experimental data in the single-phase region. It is particularly true for the P26 cases (Figure 2.13) where a large range of subcooled conditions in the single-phase region was covered.

Regarding the P14 cases (Figure 2.12), very few measurements are available outside of the boiling region. However we can see that the Gnielinski correlation seem to consistently meet the boiling measurements and follow a trend that agrees with the experimental data.

On the other hand, the Dittus-Boelter correlation fails to predict the wall temperature with a constant overestimation of approximately 5°C regardless of the case.

Note : The average liquid temperature at different heights was estimated using a one-dimensional energy balance before computing the local wall temperature predicted by correlations. The virtual length used for single-phase correlations was adjusted to cover the whole range of x_{eq} .

The nucleate boiling temperature predicted by Frost & Dzakowic correlation are in good agreement with the experimental observations where we saw the wall temperature stabilization. The prediction is better for the P26 cases than for the P14 cases where an underestimation of 1°C is observed. We can also note that the measurements are more dispersed for the P14 cases and span over a range of more than 1°C around the average temperature.

Those comparisons are comforting the consistency of the wall temperature database which correspond to traditional behavior of wall to fluid heat transfer in both single-phase and boiling two-phase regimes.

2.6 CONCLUSIONS

The DEBORA database is a very rich source of experimental insights for boiling flows representative of PWR industrial conditions. The large range of control parameters that was covered during the tests also is encouraging regarding the variety of flow regimes that can occur in PWR conditions.

After a finer analysis of the data, in the continuation of the work of Cubizolles [22], Manon [79] and Guéguen [44], we concluded that:

- The test matrix unfortunately shows that very few series were covered with both bi-optical probe (C3000) and thermocouples (C800) measurements, limiting the availability of a full boiling database to the series G2P26W16 and G2P14W16.
- Small but significant errors on the reported outlet quality could be observed when compared to a one-dimensional energy balance based on the control parameters (Table 2.5).
- Good agreement was found between the void fraction measurements with the mono (C2900) and bi-optical probe (C3000), which comforts the validity of the acquired data in close flow conditions.
- Extension of the C2900 data to estimate bubble diameter and interfacial area concentration using Eq. 2.8 to compute vapor velocity was acceptable in subcooled conditions but showed increasing underestimations in the saturated region (Figures 2.7b and 2.9b).
- Void fraction measurements in the G2P14W16 series showed a particular behavior with a peak value moving from the wall to the bulk as the inlet temperature increases.
- Bubble diameter measurements clearly exhibited coalescence phenomena when leaving the wall with a maximum value reached at $r/R \approx 0.6$ before decreasing under condensation and / or break-up (Figure 2.7c). It was also observed that measurements closest to the wall were nearly constant among a given test series regardless of the inlet temperature.
- Liquid temperature can overcome the saturation temperature for the hottest cases close to the wall ($T_L - T_{sat} \approx 0.1^\circ\text{C}$) and flattens at the bulk with a subcooling roughly around 0.5°C .
- Wall temperature measurements followed a coherent linear profile in the single-phase region before stabilizing when boiling starts, which was further reproduced by comparison with one-dimensional correlations. Measurements were also overlapping each other when plotted versus the local quality, confirming the transposition between change of inlet temperature and axial translation of the measurement section.
- Reconstruction of the applied wall heat flux in the experiments by merging the values from very close C3000 and C800 cases (Table 2.6) suggested that the heat flux values provided in the measurements were too large by 5% to 8%. Such a large difference is surprising and could partially be explained by the small change of operating conditions between C3000 and C800 cases.

At last, the different evaluations conducted over the chosen experiments have reasonably validated the consistency and coherency of the measurements. Further comparisons with NEPTUNE_CFD simulations will be conducted using the experimental results of the G2P26W16 series. **Still, we keep in mind that an error of a few % is possible on ϕ_w .**

3

NEPTUNE_CFD SIMULATIONS OF DEBORA CASES

Contents

3.1	Introduction	29
3.2	Simulation Setup	29
3.3	Mesh Sensitivity Study	30
3.4	C800 Cases Simulations : Thermal Measurements	31
3.4.1	High Subcooling Cases	31
3.4.2	Low Subcooling Cases	32
3.4.3	Saturated Cases	33
3.5	C3000 Cases Simulations : Topology Measurements	34
3.5.1	Subcooled Boiling Cases	34
3.5.2	Saturated Boiling Cases	35
3.6	Simulations Sensitivity Tests	36
3.6.1	Sensitivity to Wall Heat Flux Correction	36
3.6.2	Influence of a Wall Boiling Parameter : the Nucleation Site Density	38
3.7	Conclusion	40

3.1 INTRODUCTION

Due to the large amount of measurements along with its scaling conditions with PWR flows, the DEBORA cases have been often used for validation of multiphase simulation tools, from simple 1D / 2D codes [44, 61, 79] to CFD softwares [6, 45, 68, 89, 103], helping to conduct separate validation and comparison of several modeling aspects involved in such codes (interfacial heat and momentum transfer, turbulence, interfacial area transport, etc.).

In this Chapter, we present neptune_cfd simulations of the DEBORA experiment. The objective is to assess the current modeling of the code for dispersed two-phase boiling flows. To do so, we will simulate cases from the different campaigns of the DEBORA database (C800 and C3000) to conduct comparisons of void fraction, bubble diameter, vapor velocity, liquid temperature and wall temperature profiles.

As identified in Chapter 2, our focus will be on cases from the G2P26W16 series, since they provide the most extensive set of measurements in very close operating conditions.

3.2 SIMULATION SETUP

Since the geometry of the DEBORA experiment presents an axisymmetry, we simplify the simulation setup in order to realize a 2D axisymmetric computation. The computational domain consists of a 1° angular section of radius $R = 9.6$ mm and 3.85 m length (Figure 3.1).

The boundary conditions are:

- Uniform heat flux for $0.2 \text{ m} \leq z \leq 3.5 \text{ m}$;
- Adiabatic wall for $z < 0.2 \text{ m}$ and $z > 3.7 \text{ m}$;
- Uniform outlet pressure ;
- Uniform liquid inlet velocity and temperature ;

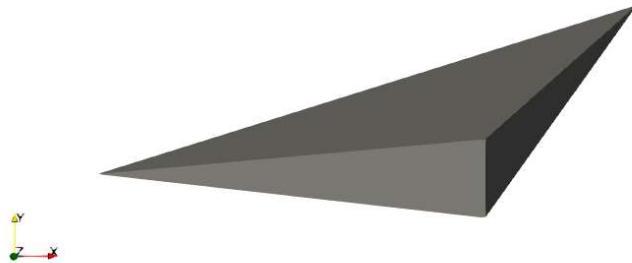


Figure 3.1: View of the computational domain.

- Symmetry condition on remaining faces.

The inlet section before heating is approximately $10D_h$ long and the extracted radial profile for comparisons is located at the end of the heating length. The angular section consists of 1 mesh while radial and axial direction are uniformly discretized. Four meshes are considered, presented on Table 3.1 and Figure 3.2.

Mesh name	M1	M2	M4	M8
Number of cells (radial \times axial)	10×100	20×200	40×400	80×800

Table 3.1: Mesh parameters

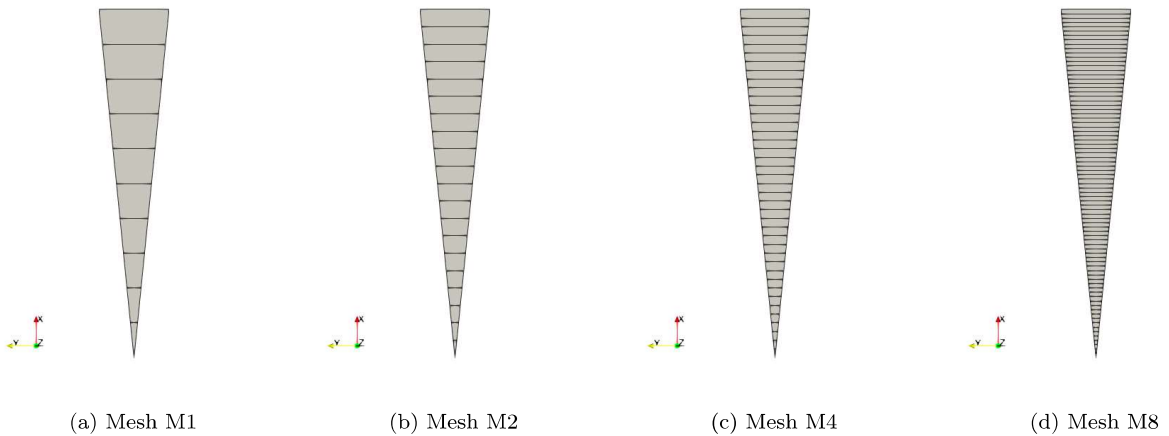


Figure 3.2: View of the radial meshes.

The computation runs using the transient solver of NCFD for a long enough physical time ensuring temporal stabilization and convergence of the results.

Note : First simulated case was simulated up to a physical time of 40 s, ensuring the time-convergence. Further simulations used this first case as a restart point, allowing to reach time-convergence in less than 10 s when changing boundary conditions.

3.3 MESH SENSITIVITY STUDY

On Figure 3.3, we present simulation results for the 4 meshes (Table 3.1) of the case 30G2P26W16Te66.6.

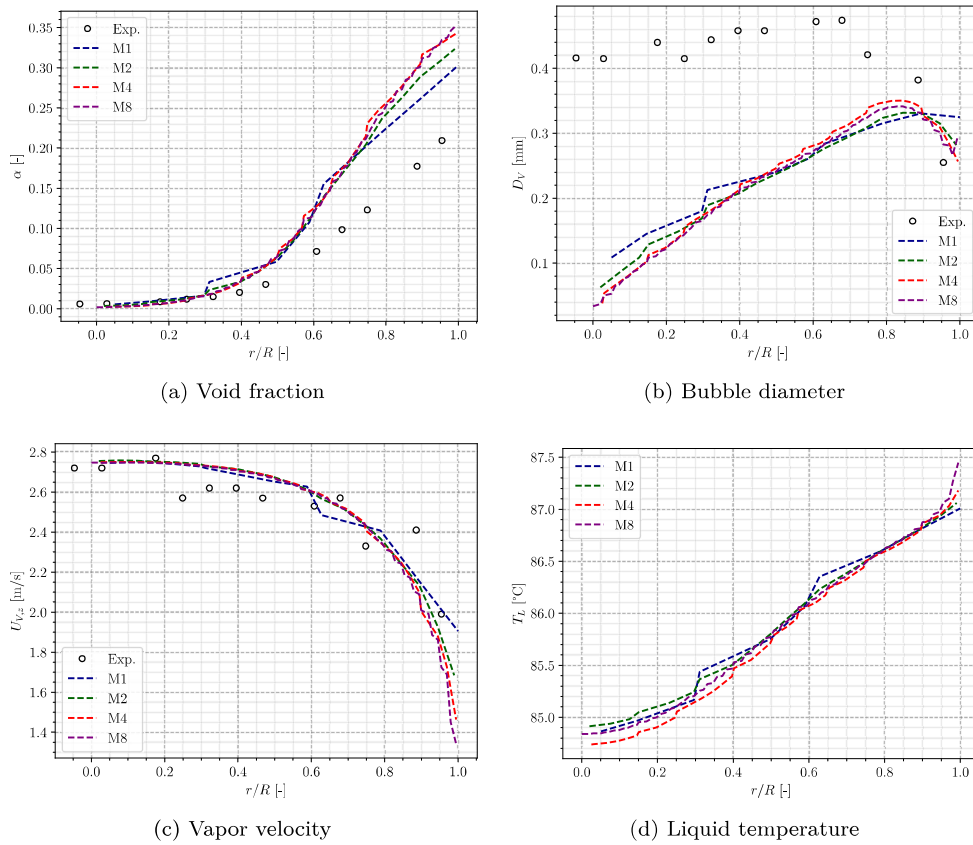


Figure 3.3: Mesh sensitivity study for 30G2P26Te66.6 case

We see that the different meshes provide similar results for the void fraction, bubble diameter, vapor velocity and liquid temperature. This is particularly true for the M4 and M8 meshes, allowing to assume that an acceptable grid convergence is reached with the M4 mesh. **Therefore, further simulations will be conducted using the M4 mesh.**

Remark : One of the most remarkable impact of the mesh concerns the liquid temperature in the wall-adjacent cell. As the mesh refines, the strong temperature gradient at the wall is logically better captured, inducing a net rise in the liquid temperature when $r/R \rightarrow 1$.

3.4 C800 CASES SIMULATIONS : THERMAL MEASUREMENTS

In this Section, we focus our attention on cases from the 8G2P26W16 series to assess liquid and wall temperature predictions. We sub-divide the case in three parts depending on the degree of subcooling at the outlet in order to cover both single-phase and fully boiling cases.

3.4.1 High Subcooling Cases

We start by simulating cases 8G2P26W16Te31.5 and Te44.9 which both have an outlet quality $x_{eq,out} < -0.25$, meaning that the fluid remains in its liquid phase along nearly the entire heating length. Results obtained for those cases are presented on Figure 3.4.

The liquid temperature profiles are fairly reproduced with the experimental parabolic shape correctly captured along with quite precise prediction of the temperature values in the bulk (Figure 3.4a). Still, we note that an overestimation of the liquid temperature near the wall and a small underestimation (less than 1°C) when approaching the center of the pipe.

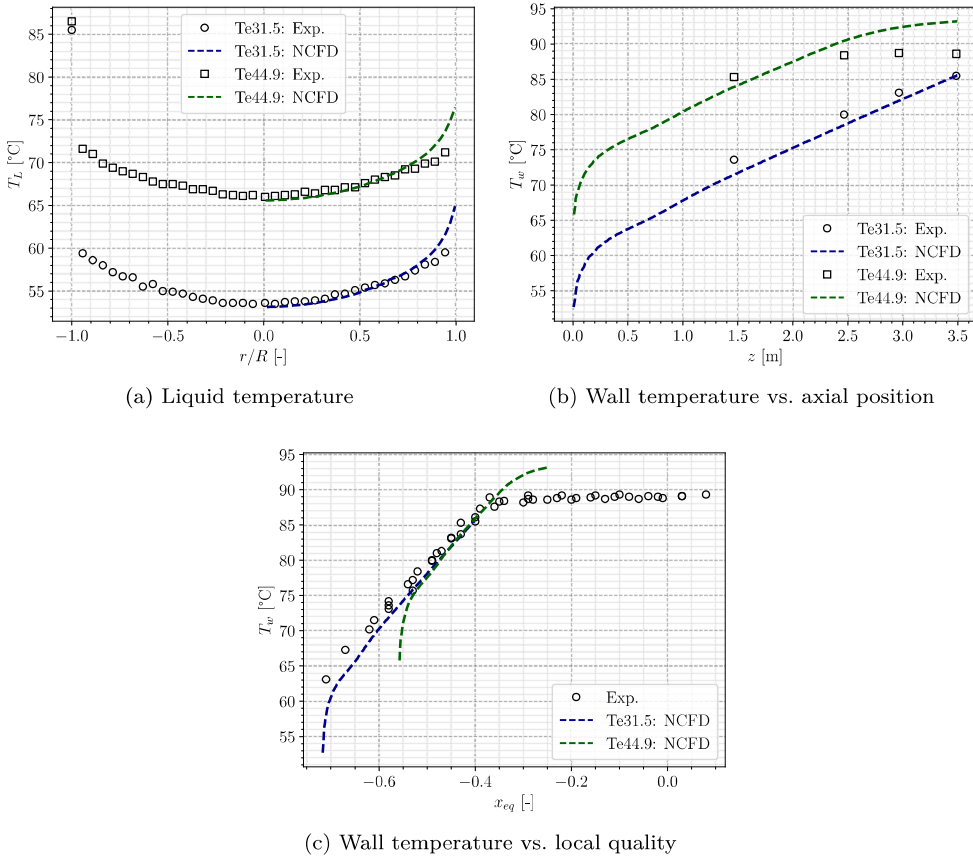


Figure 3.4: Simulation results for cases 8G2P26W16Te31.5 & Te44.9

Wall temperature predictions in the single-phase region present a good agreement with the experimental measurements along the axial positions (Figure 3.4b). This is further verified by transposition along the local quality x_{eq} (Figure 3.4c) by gathering all the measurements from the 8G2P26W16 campaign, showing an average error of approximately 1°C up to $x_{eq} \approx -0.5$.

Those comparisons highlight the validation of the code for the single-phase flow part, implying that **the local liquid heat transfer coefficient (Eq. 1.35) is correctly computed along with a good heat transport along the radial direction.**

3.4.2 Low Subcooling Cases

Next cases to be simulated are 8G2P26W16Te55.7 and Te61.5. Their outlet quality is closer to saturation with $x_{eq,out} \geq -0.1$ and thus present a subcooled boiling region during a significant portion of the heating length. However, the bulk flow is expected to stay fully liquid in those conditions (Figure 2.7a). The results are presented of Figure 3.5.

Liquid temperature profiles (Figure 3.5a) are similar to those of the high subcooling cases (Figure 3.4a). The parabolic shape of the measurements is reasonably reproduced, with liquid temperature values close to the experiment. The same discrepancies are observed, namely a overestimation close to the wall and a small underestimation at the center (also lower than 1°C).

However, the wall temperature start to show significant discrepancies with the measurements (Figure 3.5b). The deviation from the linear profile observed in the pure-single phase region towards a stabilization corresponding to the boiling regime fails to be reproduced (Figure 3.5c). First, the temperature plateau appears to start later than the experiment (around $x_{eq} \approx -0.3$ for the simulations contrary to $x_{eq} \approx -0.4$ for the experiments) and further reaches a wall temperature up to 6°C above the measurements.

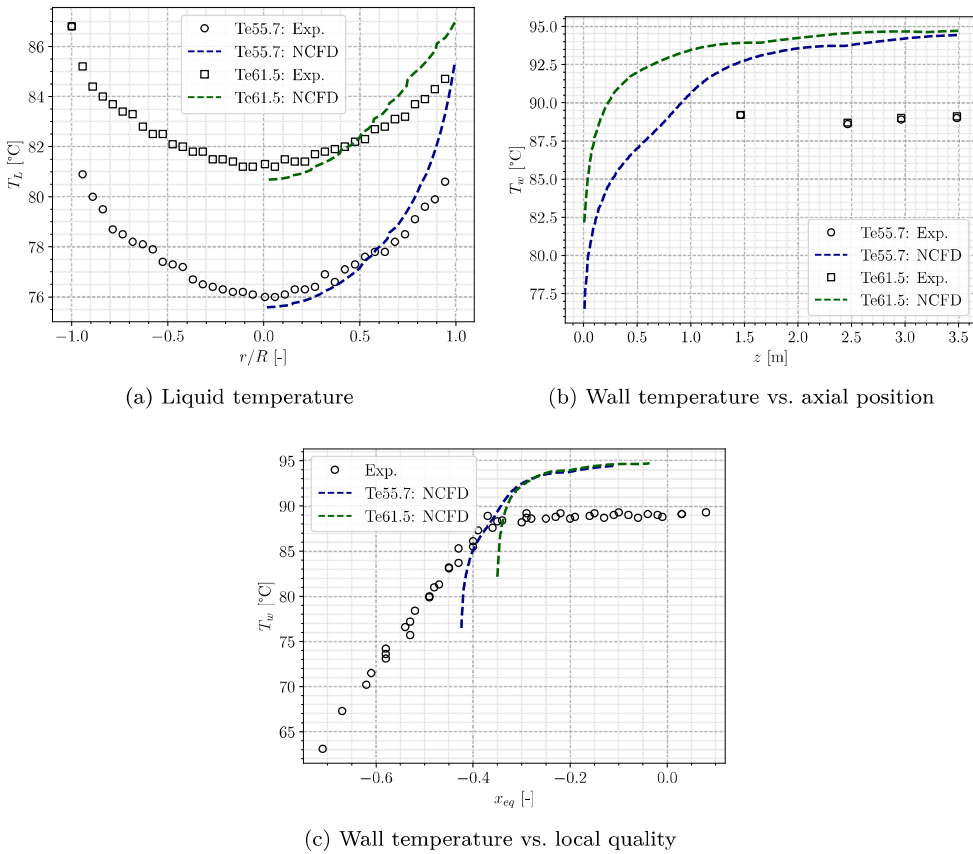


Figure 3.5: Simulation results for cases 8G2P26W16Te55.7 & Te61.5

Albeit the liquid temperature seems correctly distributed along the radial direction in the subcooled boiling region (also meaning that any amount of vapor potentially produced at the wall is correctly re-condensed), the wall temperature behavior significantly deviates from the experiments both by missing the ONB and exhibiting a too large superheat in the boiling region. **This consequently casts interrogations towards the modeling of the wall temperature in the code, which is a result of the wall boiling model (Section 1.5).**

3.4.3 Saturated Cases

Finally, we focus on saturated cases 8G2P26W16Te66.6 and Te70.3, both having an outlet quality $x_{eq,out} > 0$. Under those operating conditions, uncondensed vapor is present in the bulk flow (Figure 2.7a). Results of the simulation sfor those cases are presented on Figure 3.6.

Contrary to previous observations in subcooled cases, the liquid temperature profiles (Figure 3.6a) are overestimated ($\approx +0.6^\circ\text{C}$) over the whole radial section for both cases. The shape exhibited are however similar to the experiments, with a flattening of the liquid temperature for the Te70.3 case.

In those conditions, boiling starts immediately at the beginning of the heated length. Therefore, wall temperature is expected to rapidly stabilize to the boiling temperature, which is actually what happens in the simulations (Figure 3.6b)). As previously noted for the low subcooling cases, the wall temperature during boiling is overestimated by approximately 6°C .

Those saturated cases are confirming that **the boiling model fails to predict the wall temperature.**

Remark : The small yet observed global overestimation of the liquid temperature may be a consequence of a either a too large condensation or interfacial area concentration (*i. e.* small bubble diameter).

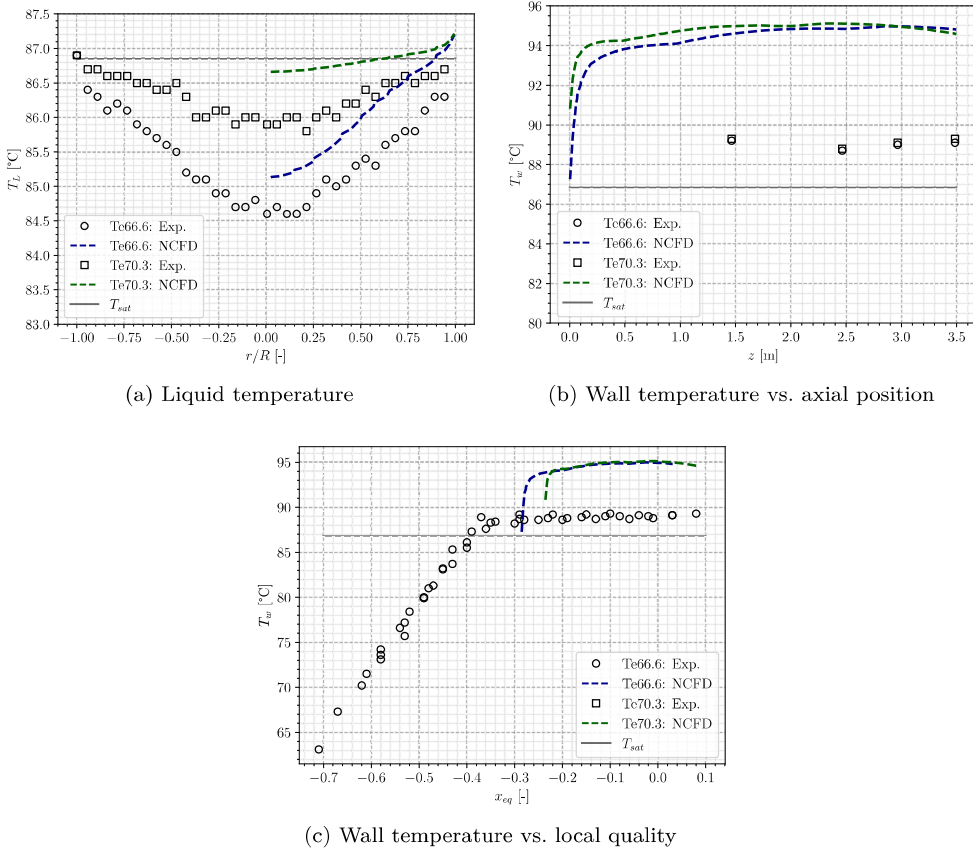


Figure 3.6: Simulation results for cases 8G2P26W16Te66.6 & Te70.3

3.5 C3000 CASES SIMULATIONS : TOPOLOGY MEASUREMENTS

Now that comparisons with thermal measurements have been conducted, we move to assessment of core flow topology predictions by the code. Based on results from the 30G2P26W16 campaign, we will compare the predictions of the void fraction, the bubble diameter and the vapor velocity at the end of the heating length. We will separately focus on subcooled boiling and saturated cases.

3.5.1 Subcooled Boiling Cases

Subcooled cases 30G2P26W16Te62 and Te64 are simulated. They both have an outlet quality $x_{eq,out} \leq 0$ with pure liquid at the center of the test section, but present significant void fraction when approaching the wall (Figure 2.7a). Results of the NEPTUNE_CFD Simulations are presented on Figure 3.8.

The void fraction (Figure 3.7a) appears globally overestimated over the whole radial section, with a difference $\alpha_{CFD} - \alpha_{exp} \approx 10\%$ at the wall. However the results seem to match the very low void fractions region ($\alpha < 3\%$) and finds a pure liquid flow roughly at the same radial position as the measurements ($r/R \approx 0.5$ and 0.3 for Te62 and Te64 cases respectively).

On the other hand, the bubble diameter (Figure 3.7b) is largely underestimated by vanishing rapidly when $r/R < 0.9$ which is not observed experimentally. Measurements contrarily show a roughly constant bubble diameter after a small increase. The simulations yet present an acceptable agreement with the experiments near the wall and even present a slight growth of the bubble diameter before its immediate decrease. **Such a discrepancy combined to a too large void fraction points towards an erroneous estimation of bubble break-up and / or condensation.**

The vapor velocity profiles (Figure 3.7c) are in accordance with the DEBORA measurements, both in the values and profile shape. **This may be supporting the evaluation of the interfacial momentum transfer determining the drift velocity between liquid and vapor.**

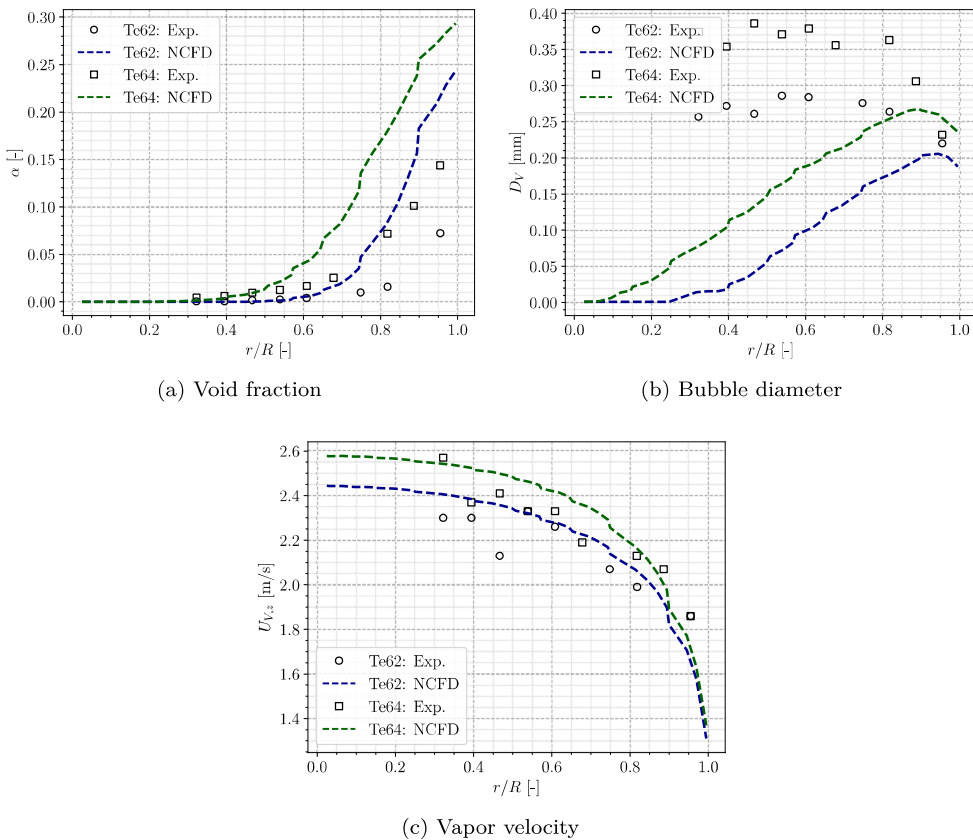


Figure 3.7: Simulation results for cases 30G2P26W16Te62 & Te64

Remark : The interfacial momentum terms (Subsection 1.3.2) also depend on the local void fraction and bubble diameter, meaning that achieving a correct velocity profile while having an erroneous void fraction and bubble diameter does not ensure the validation of the interfacial forces by itself. However, the difference in vapor velocity from one case to another is coherent with the experiments, which at least implies a correct sensitivity to the local thermal-hydraulics conditions.

3.5.2 Saturated Boiling Cases

Next we simulate two saturated cases that experimentally present a non-zero void fraction at the tube center : cases 30G2P26W16Te66 and Te70. Results are presented of Figure 3.8.

Similar to the subcooled cases, the void fraction (Figure 3.8a) is overestimated over the whole section. Case Te66 presents a wall overestimation of approximately 10% as for the subcooled simulations (Figure 3.7a) and matches the radial position where $\alpha \approx 0$. On the contrary, case Te70 is largely overestimated over the whole section, which can be explained because the liquid temperature is close to saturation, strongly limiting the impact of condensation.

Bubble diameter (Figure 3.8b) for the Te66 case behaves close to the subcooled cases, with a large overestimation under the sharp decrease when $r/R < 0.8$. However, case Te70 presents a different profile with a larger growth in bubble diameter nearly matching maximum experimental value at $r/R \approx 0.6$, but then decreases too rapidly. Recalling thermal results for the 8G2P26W16Te70.3 case presenting similar operating conditions (Figure 3.6a), $r/R \approx 0.6$ corresponds to the radial position where the computed liquid temperature becomes lower than saturation temperature, enabling condensation to occur. This tends to indicate that **condensation may be responsible for most of the bubble diameter underestimation in the sub-cooled region**. On the contrary, coalescence and break-up terms alone seem to be able to reproduce the bubble diameter increase before condensation starts.

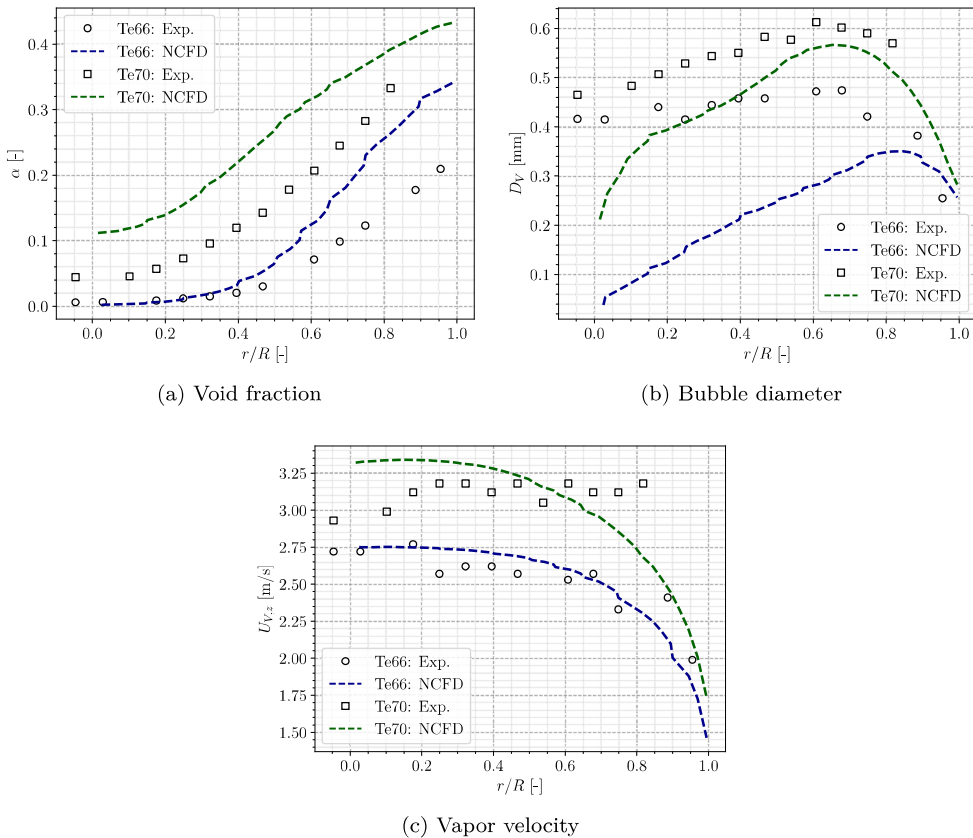


Figure 3.8: Simulation results for cases 30G2P26W16Te66 & Te70

Finally, vapor velocity (Figure 3.8c) is correctly reproduced for the Te66 case while the Te70 simulation do not reproduce the plateau observed in the measurements by keeping a parabolic profile from which the experiment deviates. The velocity magnitude achieved for the Te70 case are however coherent with the experiments.

3.6 SIMULATIONS SENSITIVITY TESTS

In this section, we perform two sensitivity tests for the CFD results presented in Sections 3.4 and 3.5.

3.6.1 Sensitivity to Wall Heat Flux Correction

As observed in previous results, the simulations for saturated cases showed simultaneous overestimation of the void fraction (Figure 3.8a), the liquid temperature (Figure 3.6a) and the wall temperature (Figure 3.6b) for topology (C3000) and thermal (C800) cases in very close experimental conditions. Such a result means that we concurrently overestimate the phase change and the liquid enthalpy, **which physically means that we injected too much energy into the system**.

Considering that the inlet conditions (liquid mass flux / velocity and temperature) are correct, we can question the value of the total heat flux applied in the simulation. This echoes the analysis conducted in Subsection 2.5.1 where assembling tests from C3000 and C800 campaign to recompute the total heat injected in the system yielded calculated heat fluxes up to 8% smaller than the given experimental value (Table 2.7).

Note : We want to insist here that this estimation was based on a "merging" of different experimental tests in similar conditions . Small differences in the control parameters (Table 2.6) between C800 and C3000 cases can partly explain the calculated heat flux "error".

In order to assess this observation, we apply a heat flux correction for the cases 8G2P26W16Te66.6 & Te70.3 respectively associated with 30G2P26W16Te66 & Te70. Recalling Table 2.7 and acknowledging that the error may have been overestimated, we apply the correction showed in Table 3.2.

Case name	Initial ϕ_w [kW/m ²]	Correction [%]	Corrected ϕ_w [kW/m ²]
30G2P26W23Te66 and 8G2P26W16Te66.6	73.9	-4%	70.94
30G2P26W23Te70 and 8G2P26W16Te70.3	73.9	-6%	69.47

Table 3.2: Corrected heat fluxes applied in the simulations

The results for each case are compared to the initial heat flux value on Figure 3.9 and Figure 3.10 for C800 and C3000 cases respectively.

3.6.1.1 Thermal Parameters

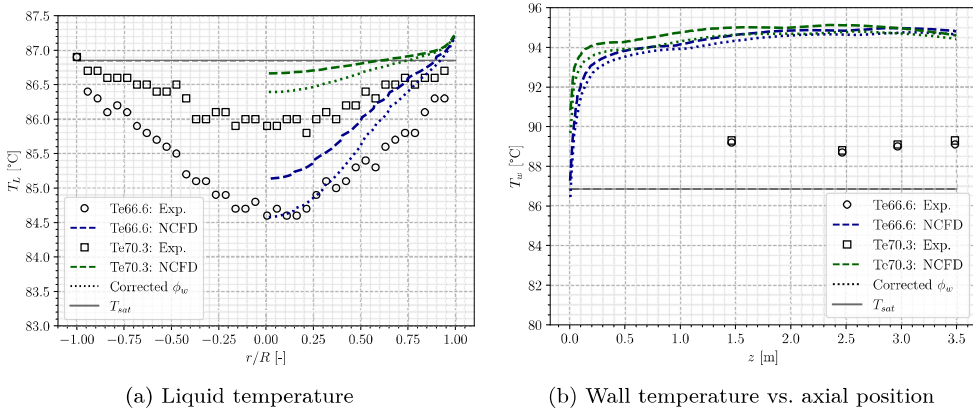


Figure 3.9: Simulation results for cases 8G2P26W16Te66.6 & Te70.3 with corrected wall heat flux

Liquid temperature (Figure 3.9a) is better predicted for both cases but is still globally overestimated. The error is nonetheless no larger than 0.5°C which is close to the measurement uncertainty of 0.2°C (Table 2.2). Case Te66.6 matches very well the bulk experimental liquid temperature with the corrected heat flux.

The wall temperature is slightly reduced at the beginning of the heated length, but stabilizes at the same value as initial simulations in the boiling region. Which leads to the same previously observed wall superheat overestimation.

3.6.1.2 Topology Parameters

Void fraction predictions are significantly enhanced for both C3000 cases (Figure 3.10a), especially regarding case Te70 which matches the experiment at the center of the tube and a maximum error $\alpha_{CFD} - \alpha_{exp} \approx 5\%$ over the whole section. Case Te66 still presents a large overestimation at the wall, but better matches bulk measurements for $r/R \leq 0.8$. However, it seems to slightly underestimate the core void fraction for $r/R \leq 0.5$.

Bubble diameter predictions are degraded when using the heat flux correction. It decreases compared to the first simulations with a decrease starting closer to the wall, further deviating from the experiments. This result could have been expected from previous observations where the strong decrease in D_V corresponds to the point where $T_L = T_{sat}$ (Figures 3.8b and 3.6a). Reducing the applied heat flux thus naturally moves this point towards the wall (Figure 3.9b).

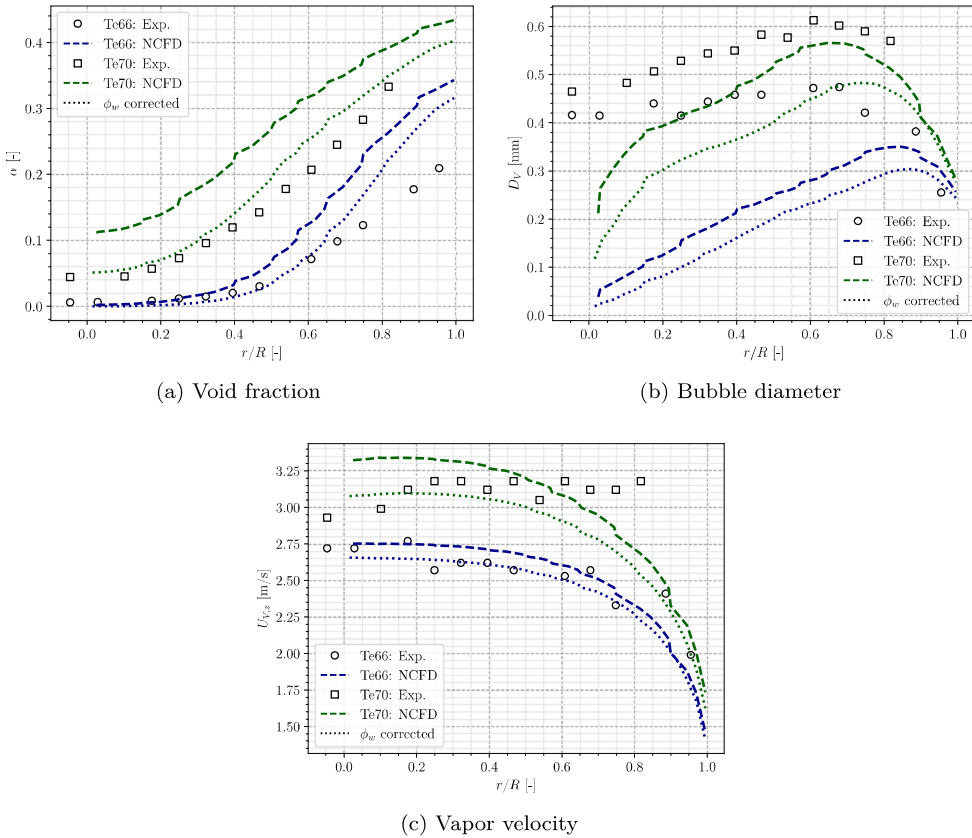


Figure 3.10: Simulation results for cases 30G2P26W16Te66 & Te70 with corrected wall heat flux

Vapor velocity profiles (Figure 3.10c) are not much impacted by the correction, with values staying relatively close to the experiment in the bulk. However, results for Te70 case even less capture the velocity plateau observed in the measurements.

3.6.2 Influence of a Wall Boiling Parameter : the Nucleation Site Density

Previous analyses showed that the wall temperature in the boiling region was badly predicted by NEPTUNE_CFD (Figures 3.5c and 3.6c) with an overestimation up to 6°C. The wall temperature is computed in the code through the model dedicated to wall boiling, namely the "Heat Flux Partitioning" model (Section 1.5).

This model involves the evaluation many different physical parameters that requires the use of correlations. For instance, the "nucleation site density" (N_{sit} , Eq. 1.36) which controls the number of bubbles that can be generated per unit of area, is evaluated using the law of Lemmert & Chawla [71] (Eq. 1.37) that only depends on the wall superheat $\Delta T_w = T_w - T_{sat}$. More recent correlations dedicated to N_{sit} evaluation have been developed since and notably include of other physical parameters such as pressure or contact angle [3, 50, 74, 136].

To test the CFD results sensitivity to the wall boiling modeling, we conduct simulations of the 8G2P26W16Te55.7 case while changing the N_{sit} correlation. This case covers a local quality range that includes single phase and boiling part (Figure 3.5c). Three nucleation site density correlations are tested:

- Lemmert & Chawla [71] (Eq. 1.37) ;
- Hibiki & Ishii [50] (Eq. 6.5) ;
- Li *et al.* [74] (Eq. 6.11).

The difference between the simulations results are presented on Figure 3.11 along with the different fluxes (liquid convection $\phi_{c,L}$, phase change ϕ_e , quenching ϕ_q and vapor convection $\phi_{c,V}$).

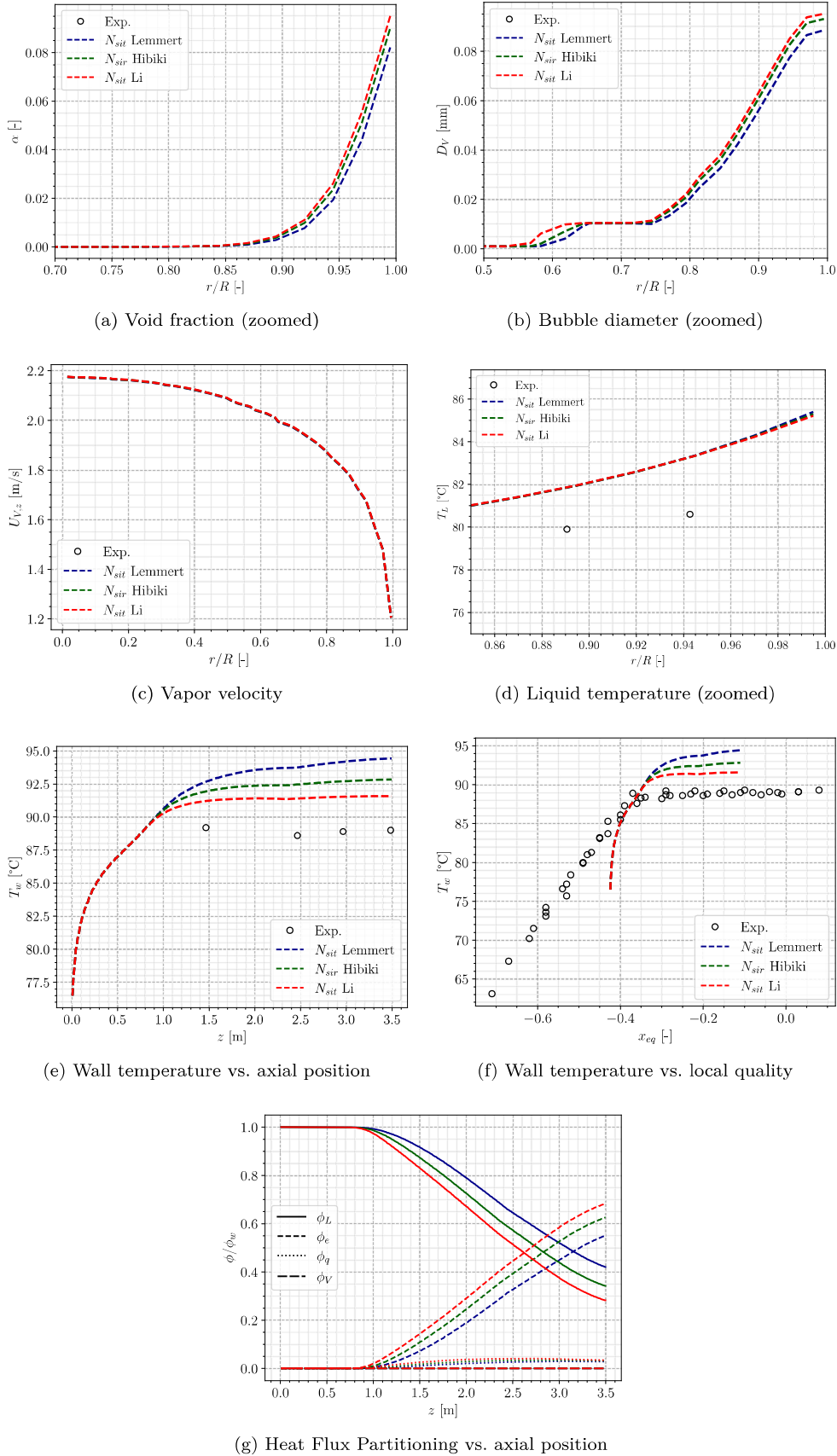


Figure 3.11: Simulation results for case 8G2P26W16Te55.7 using different nucleation site density correlations

The nucleation site density modification induces very small variations over the bulk quantities (Figures 3.11a to 3.11d). The only observable differences lie very close to the wall with an absolute void fraction

change of 1.5% and bubble diameter change less than 0.01 mm. However, the computed heat fluxes (Figure 3.11g) show large difference between the three cases, with an evaporation heat flux enhanced by more than 15% by changing from Lemmert & Chawla to Li *et al.* formulation. The absence of such a difference in the bulk means that models controlling the bulk thermodynamic equilibrium (*e.g.* condensation) rapidly compensate changes in the heat flux partitioning to reach the very similar distribution between α and T_L .

Note : This "compensating" effect of the bulk models in CFD computations when changing the wall Heat Flux Partitioning has also been noted in other works such as in Gilman & Baglietto [40] or Montout [89].

Contrary to bulk values, the wall temperature obtained in the simulations is significantly modified (Figures 3.11e and 3.11f) with an error reduction regarding the experimental measurements. Results using Li *et al.* correlation overestimates the wall temperature by 2.5°C versus up to 6°C for the first simulations. This results is probably due to the increase in evaporation heat flux ϕ_e , thus leaving less heat to be transmitted through convection and reduces the wall temperature.

Remark : The very small amount of quenching heat flux ϕ_q (Figure 3.11g) is surprising. The transient conduction induced by bubbles movements is expected to be larger because PWR-like conditions present a large number of tiny bubbles on the surface that can slide over long distances [65, 80].

3.7 CONCLUSION

This Chapter has investigated the modeling of dispersed boiling flows implemented in NEPTUNE_CFD (Chapter 1) based on simulations of the DEBORA experiment (Chapter 2). At this point, the main conclusions are:

- The single-phase flow region correctly matches the experiments, both regarding liquid and wall temperature (maximum error of approx. 1°C).
- Boiling region is hardly reproducing every measured parameters in the experiments. A good agreement is observed for vapor velocity and liquid temperature for subcooled flows. Significant discrepancies are however present for void fraction (overestimation), bubble diameter (underestimation) and wall temperature (overestimation).
- Condensation is likely to have an important impact in the bubble diameter underestimation, since its too strong decrease coincides with radial position where $T_L = T_{sat}$.
- Interfacial area transport equation seem to be able to reproduce coalescence effects in the absence of subcooled liquid / condensation.
- Testing a heat flux correction showed that a much greater agreement on the void fraction and liquid temperature could be achieved for saturated cases by diminishing ϕ_w by roughly 5%.
- Wall temperature appears to be sensitive to the closure laws involved in the Heat Flux Partitioning that models for the wall boiling phenomenon. This is not the case for the bulk properties that are left nearly unchanged.
- The wall boiling model predicts a very low quenching flux which appears surprising in such flow conditions.

All in all, these results are highlighting the difficulty of reaching a precise modeling of the multiple physical phenomena at stake in dispersed boiling flows. Despite the absolute discrepancies, the current modeling shows an encouraging behavior in the bulk (void fraction and liquid temperature shapes, coalescence / break-up / condensation impact, etc.). This could benefit from further work to precisely model the interfacial heat transfers in the flow along with bubble population quantification. Approaches considering polydispersed population of bubbles such as the iMUSIG model [krepper_2008] could be of interest in that prospect.

On the other hand, the modeling of wall boiling appears to be somewhat old-fashioned due to the use of old closure laws and based on a simple formulation of the Heat Flux Partitioning. In the frame of advancing towards local predictions of the Critical Heat Flux, it seems natural to be looking for a finer and more extensive modeling of the wall boiling.

In that regard, the next part of this manuscript will be dedicated to an investigation and construction of a new Heat Flux Partitioning model. The goal being to account for more physical phenomena at the wall (bubble sliding, interactions, etc.) along with reassessing some of the closure laws required in the formulation, with systematic comparison to experiments when possible.

BIBLIOGRAPHY

- [1] Rouhollah Ahmadi, Tatsuya Ueno, and Tomio Okawa. “Bubble dynamics at boiling incipience in subcooled upward flow boiling”. In: *International Journal of Heat and Mass Transfer* 55.1 (Jan. 15, 2012), pp. 488–497. ISSN: 0017-9310. DOI: [10.1016/j.ijheatmasstransfer.2011.09.050](https://doi.org/10.1016/j.ijheatmasstransfer.2011.09.050).
- [2] T. R. Auton. “The lift force on a spherical body in a rotational flow”. In: *Journal of Fluid Mechanics* 183 (Oct. 1987). Publisher: Cambridge University Press, pp. 199–218. ISSN: 1469-7645, 0022-1120. DOI: [10.1017/S002211208700260X](https://doi.org/10.1017/S002211208700260X).
- [3] Nilanjana Basu, Gopinath R. Warrier, and Vijay K. Dhir. “Wall Heat Flux Partitioning During Subcooled Flow Boiling: Part II—Model Validation”. In: *Journal of Heat Transfer* 127.2 (Mar. 15, 2005), pp. 141–148. ISSN: 0022-1481. DOI: [10.1115/1.1842785](https://doi.org/10.1115/1.1842785).
- [4] Nilanjana Basu, Gopinath R. Warrier, and Vijay K. Dhir. “Wall Heat Flux Partitioning During Subcooled Flow Boiling: Part 1—Model Development”. In: *Journal of Heat Transfer* 127.2 (Mar. 15, 2005), pp. 131–140. ISSN: 0022-1481. DOI: [10.1115/1.1842784](https://doi.org/10.1115/1.1842784).
- [5] Berne. “Analyse critique des modèles d’auto vaporisation utilisés dans le calcul des écoulements diphasiques en conduites”. PhD thesis. Châtenay-Malabry, Ecole centrale de Paris, 1983.
- [6] D. Bestion et al. “Review of Available Data for Validation of Nuresim Two-Phase CFD Software Applied to CHF Investigations”. In: *Science and Technology of Nuclear Installations* 2009 (Oct. 14, 2008). Publisher: Hindawi, e214512. ISSN: 1687-6075. DOI: [10.1155/2009/214512](https://doi.org/10.1155/2009/214512).
- [7] J Borée, G. Charnay, J. Fabre, D. Legendre, and J. Magnaudet. *Ecoulements diphasiques eau-vapeur avec changement de phase*. Technical Report. Toulouse: IMFT - Interface, 1992.
- [8] V. M. Borishanskii, G. I. Bobrovich, and F. P. Minchenko. “Heat transfer from a tube to water and to ethanol in nucleate pool boiling”. In: *Problems of Heat Transfer and Hydraulics of Two-Phase Media*. Elsevier, 1969, pp. 85–106.
- [9] R. W. Bowring. *Physical model, based on bubble detachment, and calculation of steam voidage in the sub-cooled region of a heated channel*. HPR-10. Institutt for Atomenergi (Norway). OECD Halden Reaktor Prosjekt, Dec. 1, 1962.
- [10] Mattia Bucci, Jacopo Buongiorno, and Matteo Bucci. “The not-so-subtle flaws of the force balance approach to predict the departure of bubbles in boiling heat transfer”. In: *Physics of Fluids* 33.1 (Jan. 2021). Publisher: American Institute of Physics, p. 017110. ISSN: 1070-6631. DOI: [10.1063/5.0036956](https://doi.org/10.1063/5.0036956).
- [11] Lubomír Bureš and Yohei Sato. “On the modelling of the transition between contact-line and microlayer evaporation regimes in nucleate boiling”. In: *Journal of Fluid Mechanics* 916 (June 2021). Publisher: Cambridge University Press. ISSN: 0022-1120, 1469-7645. DOI: [10.1017/jfm.2021.204](https://doi.org/10.1017/jfm.2021.204).
- [12] In-Cheol CHU, Hee Cheon NO, and Chul-Hwa SONG. “Bubble Lift-off Diameter and Nucleation Frequency in Vertical Subcooled Boiling Flow”. In: *Journal of Nuclear Science and Technology* 48.6 (June 1, 2011). Publisher: Taylor & Francis _eprint: <https://www.tandfonline.com/doi/pdf/10.1080/18811248.2011.9711780>. pp. 936–949. ISSN: 0022-3131. DOI: [10.1080/18811248.2011.9711780](https://doi.org/10.1080/18811248.2011.9711780).
- [13] Deqi Chen, Liang-ming Pan, and Song Ren. “Prediction of bubble detachment diameter in flow boiling based on force analysis”. In: *Nuclear Engineering and Design* 243 (Feb. 1, 2012), pp. 263–271. ISSN: 0029-5493. DOI: [10.1016/j.nucengdes.2011.11.022](https://doi.org/10.1016/j.nucengdes.2011.11.022).
- [14] J. C. Chen. “Correlation for Boiling Heat Transfer to Saturated Fluids in Convective Flow”. In: *Industrial & Engineering Chemistry Process Design and Development* 5.3 (July 1, 1966). Publisher: American Chemical Society, pp. 322–329. ISSN: 0196-4305. DOI: [10.1021/i260019a023](https://doi.org/10.1021/i260019a023).
- [15] Zhihao Chen, Atsushi Haginiwa, and Yoshio Utaka. “Detailed structure of microlayer in nucleate pool boiling for water measured by laser interferometric method”. In: *International Journal of Heat and Mass Transfer* 108 (May 1, 2017), pp. 1285–1291. ISSN: 0017-9310. DOI: [10.1016/j.ijheatmasstransfer.2017.01.003](https://doi.org/10.1016/j.ijheatmasstransfer.2017.01.003).

- [16] Zhihao Chen, Xiaocheng Hu, Kang Hu, Yoshio Utaka, and Shoji Mori. "Measurement of the microlayer characteristics in the whole range of nucleate boiling for water by laser interferometry". In: *International Journal of Heat and Mass Transfer* 146 (Jan. 1, 2020), p. 118856. ISSN: 0017-9310. DOI: [10.1016/j.ijheatmasstransfer.2019.118856](https://doi.org/10.1016/j.ijheatmasstransfer.2019.118856).
- [17] Han Chi-Yeh and Peter Griffith. "The mechanism of heat transfer in nucleate pool boiling—Part I: Bubble initiation, growth and departure". In: *International Journal of Heat and Mass Transfer* 8.6 (June 1, 1965), pp. 887–904. ISSN: 0017-9310. DOI: [10.1016/0017-9310\(65\)90073-6](https://doi.org/10.1016/0017-9310(65)90073-6).
- [18] SW Churchill. "Friction Factor Spans All Fluid-Flow Regimes". In: *Chemical Engineering* 84 (1977), pp. 91–92.
- [19] Robert Cole. "Bubble frequencies and departure volumes at subatmospheric pressures". In: *AIChE Journal* 13.4 (1967). _eprint: <https://onlinelibrary.wiley.com/doi/pdf/10.1002/aic.690130434>, pp. 779–783. ISSN: 1547-5905. DOI: [10.1002/aic.690130434](https://doi.org/10.1002/aic.690130434).
- [20] Marco Colombo and Michael Fairweather. "Prediction of bubble departure in forced convection boiling: A mechanistic model". In: *International Journal of Heat and Mass Transfer* 85 (June 1, 2015), pp. 135–146. ISSN: 0017-9310. DOI: [10.1016/j.ijheatmasstransfer.2015.01.103](https://doi.org/10.1016/j.ijheatmasstransfer.2015.01.103).
- [21] M. G. Cooper and A. J. P. Lloyd. "The microlayer in nucleate pool boiling". In: *International Journal of Heat and Mass Transfer* 12.8 (Aug. 1, 1969), pp. 895–913. ISSN: 0017-9310. DOI: [10.1016/0017-9310\(69\)90154-9](https://doi.org/10.1016/0017-9310(69)90154-9).
- [22] Géraud Cubizolles. "Etude stéréologique de la topologie des écoulements diphasiques à haute pression". These de doctorat. Ecully, Ecole centrale de Lyon, Jan. 1, 1996.
- [23] D. J. Daley and D. Vere-Jones. *An Introduction to the Theory of Point Processes*. Probability and its Applications. New York: Springer-Verlag, 2003. ISBN: 978-0-387-95541-4. DOI: [10.1007/b97277](https://doi.org/10.1007/b97277).
- [24] Victor H. Del Valle and D. B. R. Kenning. "Subcooled flow boiling at high heat flux". In: *International Journal of Heat and Mass Transfer* 28.10 (Oct. 1, 1985), pp. 1907–1920. ISSN: 0017-9310. DOI: [10.1016/0017-9310\(85\)90213-3](https://doi.org/10.1016/0017-9310(85)90213-3).
- [25] Jean-Marc Delhaye. *Thermohydraulique des réacteurs*. Google-Books-ID: v8vL04U7Zt4C. EDP Sciences, Dec. 3, 2012. 527 pp. ISBN: 978-2-7598-0308-8.
- [26] Etienne Demarly. "A new approach to predicting departure from Nucleate Boiling (DNB) from direct representation of boiling heat transfer physics". Accepted: 2021-02-19T20:35:27Z ISBN: 9781237640528. Thesis. Massachusetts Institute of Technology, 2020.
- [27] F. W. Dittus and L. M. K. Boelter. "Heat transfer in automobile radiators of the tubular type". In: *International Communications in Heat and Mass Transfer* 12.1 (Jan. 1, 1985), pp. 3–22. ISSN: 0735-1933. DOI: [10.1016/0735-1933\(85\)90003-X](https://doi.org/10.1016/0735-1933(85)90003-X).
- [28] G. Duhar, G. Riboux, and C. Colin. "Vapour bubble growth and detachment at the wall of shear flow". In: *Heat and Mass Transfer* 45.7 (May 1, 2009), pp. 847–855. ISSN: 1432-1181. DOI: [10.1007/s00231-007-0287-y](https://doi.org/10.1007/s00231-007-0287-y).
- [29] Géraldine Duhar. "Croissance et détachement de bulles en paroi d'un écoulement cisaillé : étude expérimentale de l'injection et de l'ébullition nucléée". These de doctorat. Toulouse, INPT, Jan. 1, 2003.
- [30] Géraldine Duhar and Catherine Colin. "Dynamics of bubble growth and detachment in a viscous shear flow". In: *Physics of Fluids* 18.7 (July 2006). Publisher: American Institute of Physics, p. 077101. ISSN: 1070-6631. DOI: [10.1063/1.2213638](https://doi.org/10.1063/1.2213638).
- [31] Carlos E. Estrada-Pérez, Yassin A. Hassan, Bandar Alkhudhiri, and Junsoo Yoo. "Time-resolved measurements of liquid–vapor thermal interactions throughout the full life-cycle of sliding bubbles at subcooled flow boiling conditions". In: *International Journal of Multiphase Flow* 99 (Feb. 1, 2018), pp. 94–110. ISSN: 0301-9322. DOI: [10.1016/j.ijmultiphaseflow.2017.10.002](https://doi.org/10.1016/j.ijmultiphaseflow.2017.10.002).
- [32] H. K. Forster and N. Zuber. "Growth of a Vapor Bubble in a Superheated Liquid". In: *Journal of Applied Physics* 25.4 (Apr. 1954). Publisher: American Institute of Physics, pp. 474–478. ISSN: 0021-8979. DOI: [10.1063/1.1721664](https://doi.org/10.1063/1.1721664).
- [33] W Frost, G. S Dzakowic, and American Society of Mechanical Engineers. *An extension of the method for predicting incipient boiling on commercially finished surfaces*. OCLC: 459788171. New York, N.Y.: ASME, 1967.

- [34] R. F. Gaertner and J. W. Westwater. "Population of Active Sites in Nucleate Boiling Heat Transfer". In: *Chem. Eng. Progr.* Vol: 56: Symposium Ser. No. 30 (Jan. 1, 1960). Institution: General Electric Co., Schenectady, N.Y.
- [35] J. Garnier, E. Manon, and G. Cubizolles. "LOCAL MEASUREMENTS ON FLOW BOILING OF REFRIGERANT 12 IN A VERTICAL TUBE". In: *Multiphase Science and Technology* 13.1 (2001). Publisher: Begell House Inc. ISSN: 0276-1459, 1943-6181. DOI: [10.1615/MultScienTechn.v13.i1-2.10](https://doi.org/10.1615/MultScienTechn.v13.i1-2.10).
- [36] C. W. M. van der Geld. "The dynamics of a boiling bubble before and after detachment". In: *Heat and Mass Transfer* 45.7 (May 1, 2009), pp. 831–846. ISSN: 1432-1181. DOI: [10.1007/s00231-007-0254-7](https://doi.org/10.1007/s00231-007-0254-7).
- [37] Craig Douglas Gerardi. "Investigation of the pool boiling heat transfer enhancement of nano-engineered fluids by means of high-speed infrared thermography". Accepted: 2010-03-24T20:38:10Z. Thesis. Massachusetts Institute of Technology, 2009.
- [38] Craig Gerardi, Jacopo Buongiorno, Lin-wen Hu, and Thomas McKrell. "Study of bubble growth in water pool boiling through synchronized, infrared thermometry and high-speed video". In: *International Journal of Heat and Mass Transfer* 53.19 (Sept. 1, 2010), pp. 4185–4192. ISSN: 0017-9310. DOI: [10.1016/j.ijheatmasstransfer.2010.05.041](https://doi.org/10.1016/j.ijheatmasstransfer.2010.05.041).
- [39] Lindsey Anne Gilman. "Development of a general purpose subgrid wall boiling model from improved physical understanding for use in computational fluid dynamics". Accepted: 2014-12-08T18:48:48Z. Thesis. Massachusetts Institute of Technology, 2014.
- [40] Lindsey Gilman and Emilio Baglietto. "A self-consistent, physics-based boiling heat transfer modeling framework for use in computational fluid dynamics". In: *International Journal of Multiphase Flow* 95 (Oct. 1, 2017), pp. 35–53. ISSN: 0301-9322. DOI: [10.1016/j.ijmultiphaseflow.2017.04.018](https://doi.org/10.1016/j.ijmultiphaseflow.2017.04.018).
- [41] V. Gnielinski. "New equations for heat and mass transfer in the turbulent flow in pipes and channels". In: *NASA STI/Recon Technical Report A* 41 (Jan. 1, 1975). ADS Bibcode: 1975STIA...7522028G, pp. 8–16.
- [42] P. Griffith, J. A. Clark, and W. M. Rohsenow. *VOID VOLUMES IN SUBCOOLED BOILING SYSTEMS. Technical Report No. 12.* NP-6637. Massachusetts Inst. of Tech., Cambridge. Div. of Industrial Cooperation, Mar. 1, 1958.
- [43] Peng Guan, Li Jia, Liaoifei Yin, and Zetao Tan. "Bubble departure size in flow boiling". In: *Heat and Mass Transfer* 51.7 (July 1, 2015), pp. 921–930. ISSN: 1432-1181. DOI: [10.1007/s00231-014-1461-7](https://doi.org/10.1007/s00231-014-1461-7).
- [44] Jil Gueguen. "Contribution à la modélisation multidimensionnelle des écoulements bouillants convectifs en conduite haute pression pour l'application au cas des réacteurs à eau pressurisée". These de doctorat. Grenoble, Dec. 19, 2013.
- [45] Antoine Guelfi, Dominique Bestion, Marc Boucker, Pascal Boudier, Philippe Fillion, Marc Grandotto, Jean-Marc Hérard, Eric Hervieu, and Pierre Péturaud. "NEPTUNE: A New Software Platform for Advanced Nuclear Thermal Hydraulics". In: *Nuclear Science and Engineering* 156.3 (July 1, 2007). Publisher: Taylor & Francis _eprint: <https://doi.org/10.13182/NSE05-98>, pp. 281–324. ISSN: 0029-5639. DOI: [10.13182/NSE05-98](https://doi.org/10.13182/NSE05-98).
- [46] Alexandre Guion, Shahriar Afkhami, Stéphane Zaleski, and Jacopo Buongiorno. "Simulations of microlayer formation in nucleate boiling". In: *International Journal of Heat and Mass Transfer* 127 (Dec. 1, 2018), pp. 1271–1284. ISSN: 0017-9310. DOI: [10.1016/j.ijheatmasstransfer.2018.06.041](https://doi.org/10.1016/j.ijheatmasstransfer.2018.06.041).
- [47] K. E. Gungor and R. H. S. Winterton. "A general correlation for flow boiling in tubes and annuli". In: *International Journal of Heat and Mass Transfer* 29.3 (Mar. 1, 1986), pp. 351–358. ISSN: 0017-9310. DOI: [10.1016/0017-9310\(86\)90205-X](https://doi.org/10.1016/0017-9310(86)90205-X).
- [48] F. C. Gunther. "Photographic Study of Surface-Boiling Heat Transfer to Water With Forced Convection". In: *Transactions of the American Society of Mechanical Engineers* 73.2 (1951), pp. 115–123. ISSN: 0097-6822. DOI: [10.1115/1.4016160](https://doi.org/10.1115/1.4016160).
- [49] J. S. Hadamard. "Mouvement permanent lent d'une sphère liquide et visqueuse dans un liquide visqueux". In: *Comptes Rendus Hebdomadaires des Séances de l'Académie des Sciences* 155 (1911), pp. 1735–1738.

- [50] Takashi Hibiki and Mamoru Ishii. "Active nucleation site density in boiling systems". In: *International Journal of Heat and Mass Transfer* 46.14 (July 1, 2003), pp. 2587–2601. ISSN: 0017-9310. DOI: [10.1016/S0017-9310\(03\)00031-0](https://doi.org/10.1016/S0017-9310(03)00031-0).
- [51] M. Ishii. *One-dimensional drift-flux model and constitutive equations for relative motion between phases in various two-phase flow regimes*. ANL-77-47. Argonne National Lab., Ill. (USA), Oct. 1, 1977. DOI: [10.2172/6871478](https://doi.org/10.2172/6871478).
- [52] Mamoru Ishii and Takashi Hibiki. *Thermo-Fluid Dynamics of Two-Phase Flow*. New York, NY: Springer, 2011. ISBN: 978-1-4419-7984-1 978-1-4419-7985-8. DOI: [10.1007/978-1-4419-7985-8](https://doi.org/10.1007/978-1-4419-7985-8).
- [53] Mamoru Ishii and Novak Zuber. "Drag coefficient and relative velocity in bubbly, droplet or particulate flows". In: *AIChE Journal* 25.5 (1979). _eprint: <https://onlinelibrary.wiley.com/doi/pdf/10.1002/aic.690250513>. pp. 843–855. ISSN: 1547-5905. DOI: [10.1002/aic.690250513](https://doi.org/10.1002/aic.690250513).
- [54] W. H. Jens and P. A. Lottes. *Analysis of Heat Transfer, Burnout, Pressure Drop and Density Data for High-Pressure Water*. ANL-4627. Argonne National Lab., May 1, 1951. DOI: [10.2172/4421630](https://doi.org/10.2172/4421630).
- [55] R. L. Judd and K. S. Hwang. "A Comprehensive Model for Nucleate Pool Boiling Heat Transfer Including Microlayer Evaporation". In: *Journal of Heat Transfer* 98.4 (Nov. 1, 1976), pp. 623–629. ISSN: 0022-1481. DOI: [10.1115/1.3450610](https://doi.org/10.1115/1.3450610).
- [56] B. A Kader and A. M Yaglom. "Heat and mass transfer laws for fully turbulent wall flows". In: *International Journal of Heat and Mass Transfer* 15.12 (Dec. 1, 1972), pp. 2329–2351. ISSN: 0017-9310. DOI: [10.1016/0017-9310\(72\)90131-7](https://doi.org/10.1016/0017-9310(72)90131-7).
- [57] Satish G. Kandlikar and Mark E. Steinke. "Contact angles and interface behavior during rapid evaporation of liquid on a heated surface". In: *International Journal of Heat and Mass Transfer* 45.18 (Aug. 1, 2002), pp. 3771–3780. ISSN: 0017-9310. DOI: [10.1016/S0017-9310\(02\)00090-X](https://doi.org/10.1016/S0017-9310(02)00090-X).
- [58] William E. Kennel. "Local boiling of water and superheating of high pressure steam in annuli". Accepted: 2020-09-25T21:06:56Z ISSN: 2933-0025. Thesis. Massachusetts Institute of Technology, 1949.
- [59] J. F. Klausner, R. Mei, D. M. Bernhard, and L. Z. Zeng. "Vapor bubble departure in forced convection boiling". In: *International Journal of Heat and Mass Transfer* 36.3 (Feb. 1, 1993), pp. 651–662. ISSN: 0017-9310. DOI: [10.1016/0017-9310\(93\)80041-R](https://doi.org/10.1016/0017-9310(93)80041-R).
- [60] Michel Kledy. "Développement d'une méthode de mesure des champs de vitesse et de température liquide en écoulement diphasique bouillant en conditions réacteurs ou simulantes". These de doctorat. Université Grenoble Alpes (ComUE), May 30, 2018.
- [61] Michel Kledy, Fabrice François, Henda Djeridi, Stephane Barre, and Jean-Marc Delhaye. "Toward a local drift flux model for high-pressure, subcooled, convective boiling flows". In: *International Journal of Heat and Mass Transfer* 177 (Oct. 1, 2021), p. 121506. ISSN: 0017-9310. DOI: [10.1016/j.ijheatmasstransfer.2021.121506](https://doi.org/10.1016/j.ijheatmasstransfer.2021.121506).
- [62] G. Kocamustafaogullari. "Pressure dependence of bubble departure diameter for water". In: *International Communications in Heat and Mass Transfer* 10.6 (Nov. 1, 1983), pp. 501–509. ISSN: 0735-1933. DOI: [10.1016/0735-1933\(83\)90057-X](https://doi.org/10.1016/0735-1933(83)90057-X).
- [63] L. D. Koffman and M. S. Plesset. "Experimental Observations of the Microlayer in Vapor Bubble Growth on a Heated Solid". In: *Journal of Heat Transfer* 105.3 (Aug. 1, 1983), pp. 625–632. ISSN: 0022-1481. DOI: [10.1115/1.3245631](https://doi.org/10.1115/1.3245631).
- [64] Ravikishore Kommajosyula. "Development and assessment of a physics-based model for subcooled flow boiling with application to CFD". Accepted: 2021-01-05T23:15:30Z. Thesis. Massachusetts Institute of Technology, 2020.
- [65] Artyom Kossolapov. "Experimental Investigation of Subcooled Flow Boiling and CHF at Prototypical Pressures of Light Water Reactors". PhD thesis. Massachusetts Institute of Technology, 2021.
- [66] N. Kurul and Michael Z. Podowski. "MULTIDIMENSIONAL EFFECTS IN FORCED CONVECTION SUBCOOLED BOILING". In: International Heat Transfer Conference 9. Begel House Inc., 1990. ISBN: 0-89116-909-1. DOI: [10.1615/IHTC9.40](https://doi.org/10.1615/IHTC9.40).
- [67] Sir Horace Lamb. *Hydrodynamics*. Google-Books-ID: d_AoAAAAYAAJ. University Press, 1895. 632 pp. ISBN: 978-1-4086-1332-0.

- [68] Jérôme Laviéville, Nicolas Mérigoux, Mathieu Guingo, Cyril Baudry, and Stéphane Mimouni. "A Generalized turbulent dispersion model for bubbly flow numerical simulation in NEPTUNE_CFD". In: *Nuclear Engineering and Design*. 16th International Topical Meeting on Nuclear Reactor Thermal Hydraulics 312 (Feb. 1, 2017), pp. 284–293. ISSN: 0029-5493. DOI: [10.1016/j.nucengdes.2016.11.003](https://doi.org/10.1016/j.nucengdes.2016.11.003).
- [69] Dominique Legendre, Jacques Borée, and Jacques Magnaudet. "Thermal and dynamic evolution of a spherical bubble moving steadily in a superheated or subcooled liquid". In: *Physics of Fluids* 10.6 (June 1998). Publisher: American Institute of Physics, pp. 1256–1272. ISSN: 1070-6631. DOI: [10.1063/1.869654](https://doi.org/10.1063/1.869654).
- [70] Dominique Legendre and Jacques Magnaudet. "The lift force on a spherical bubble in a viscous linear shear flow". In: *Journal of Fluid Mechanics* 368 (Aug. 1998). Publisher: Cambridge University Press, pp. 81–126. ISSN: 1469-7645, 0022-1120. DOI: [10.1017/S0022112098001621](https://doi.org/10.1017/S0022112098001621).
- [71] M. Lemmert and J.M. Chawla. "Influence of flow velocity on surface boiling heat transfer coefficient". In: *Heat Transfer in Boiling*. Hemisphere. Washington D.C., 1977, pp. 236–246.
- [72] Octave Levenspiel. "Collapse of Steam Bubbles in Water". In: *Industrial & Engineering Chemistry* 51.6 (June 1, 1959). Publisher: American Chemical Society, pp. 787–790. ISSN: 0019-7866. DOI: [10.1021/ie50594a045](https://doi.org/10.1021/ie50594a045).
- [73] V. G. Levich. *Physicochemical hydrodynamics*. Prentice-Hall international series in the physical and chemical engineering sciences. OCLC: 1378432. Englewood Cliffs, N.J.: Prentice-Hall, 1962. 700 pp. ISBN: 978-0-13-674440-5.
- [74] Quan Li, Yongjun Jiao, Maria Avramova, Ping Chen, Junchong Yu, Jie Chen, and Jason Hou. "Development, verification and application of a new model for active nucleation site density in boiling systems". In: *Nuclear Engineering and Design* 328 (Mar. 1, 2018), pp. 1–9. ISSN: 0029-5493. DOI: [10.1016/j.nucengdes.2017.12.027](https://doi.org/10.1016/j.nucengdes.2017.12.027).
- [75] Z. Liu and R. H. S. Winterton. "A general correlation for saturated and subcooled flow boiling in tubes and annuli, based on a nucleate pool boiling equation". In: *International Journal of Heat and Mass Transfer* 34.11 (Nov. 1, 1991), pp. 2759–2766. ISSN: 0017-9310. DOI: [10.1016/0017-9310\(91\)90234-6](https://doi.org/10.1016/0017-9310(91)90234-6).
- [76] R.W. Lockhart and R.C. Martinelli. "Proposed Correlation of Data for Isothermal Two-Phase, Two-Component Flow in Pipes." In: *Chemical Engineering Progress* 45 (), pp. 38–48.
- [77] J. Magnaudet and I. Eames. "The Motion of High-Reynolds-Number Bubbles in Inhomogeneous Flows". In: *Annual Review of Fluid Mechanics* 32.1 (2000). _eprint: <https://doi.org/10.1146/annurev.fluid.32.1.659>. pp. 659–708. DOI: [10.1146/annurev.fluid.32.1.659](https://doi.org/10.1146/annurev.fluid.32.1.659).
- [78] Sandipan Maity. "Effect of Velocity and Gravity on Bubble Dynamics". MSc Thesis. University of California Los Angeles, 2000.
- [79] Etienne Manon. "Contribution à l'analyse et à la modélisation locale des écoulements bouillants sous-saturés dans les conditions des réacteurs à eau sous pression". These de doctorat. Châtenay-Malabry, Ecole centrale de Paris, Jan. 1, 2000.
- [80] Philippe (1970 March. "Caractérisation et modélisation de l'environnement thermohydraulique et chimique des gaines de combustible des réacteurs à eau sous pression en présence d'ébullition". These de doctorat. Aix-Marseille 1, Jan. 1, 1999.
- [81] T. Mazzocco, W. Ambrosini, R. Kommajosula, and E. Baglietto. "A reassessed model for mechanistic prediction of bubble departure and lift off diameters". In: *International Journal of Heat and Mass Transfer* 117 (Feb. 1, 2018), pp. 119–124. ISSN: 0017-9310. DOI: [10.1016/j.ijheatmasstransfer.2017.09.105](https://doi.org/10.1016/j.ijheatmasstransfer.2017.09.105).
- [82] William H McAdams. *Heat transmission*. OCLC: 683455. New York: McGraw-Hill, 1954.
- [83] Renwei Mei and J. F. Klausner. "Shear lift force on spherical bubbles". In: *International Journal of Heat and Fluid Flow* 15.1 (Feb. 1, 1994), pp. 62–65. ISSN: 0142-727X. DOI: [10.1016/0142-727X\(94\)90031-0](https://doi.org/10.1016/0142-727X(94)90031-0).
- [84] Renwei Mei and James F. Klausner. "Unsteady force on a spherical bubble at finite Reynolds number with small fluctuations in the free-stream velocity". In: *Physics of Fluids A: Fluid Dynamics* 4.1 (Jan. 1992). Publisher: American Institute of Physics, pp. 63–70. ISSN: 0899-8213. DOI: [10.1063/1.858501](https://doi.org/10.1063/1.858501).

- [85] B. B Mikic, W. M Rohsenow, and P Griffith. "On bubble growth rates". In: *International Journal of Heat and Mass Transfer* 13.4 (Apr. 1, 1970), pp. 657–666. ISSN: 0017-9310. DOI: [10.1016/0017-9310\(70\)90040-2](https://doi.org/10.1016/0017-9310(70)90040-2).
- [86] Louis Melville Milne-Thomson. *Theoretical Hydrodynamics*. Google-Books-ID: A5hRAAAAMAAJ. Macmillan and Company, limited, 1938. 590 pp.
- [87] S. Mimouni, C. Baudry, M. Guingo, J. Lavieille, N. Merigoux, and N. Mechitoua. "Computational multi-fluid dynamics predictions of critical heat flux in boiling flow". In: *Nuclear Engineering and Design*. CFD4NRS-5 299 (Apr. 1, 2016), pp. 28–36. ISSN: 0029-5493. DOI: [10.1016/j.nucengdes.2015.07.017](https://doi.org/10.1016/j.nucengdes.2015.07.017).
- [88] S. Mimouni, J. Laviéville, N. Seiler, and P. Ruyer. "Combined evaluation of second order turbulence model and polydispersion model for two-phase boiling flow and application to fuel assembly analysis". In: *Nuclear Engineering and Design*. 13th International Topical Meeting on Nuclear Reactor Thermal Hydraulics (NURETH-13) 241.11 (Nov. 1, 2011), pp. 4523–4536. ISSN: 0029-5493. DOI: [10.1016/j.nucengdes.2010.12.028](https://doi.org/10.1016/j.nucengdes.2010.12.028).
- [89] Michaël Montout. "Contribution au développement d'une Approche Prédictive Locale de la crise d'ébullition". These de doctorat. Toulouse, INPT, Jan. 21, 2009.
- [90] P. de. Munk. *Two-phase flow experiments in a 10 m long sodium heated steam generator test section*. AED-Conf-73-445-021 INIS Reference Number: 5098086. Germany, 1973, p. 2.
- [91] Tomio Okawa, Tatsuhiro Ishida, Isao Kataoka, and Michitsugu Mori. "Bubble rise characteristics after the departure from a nucleation site in vertical upflow boiling of subcooled water". In: *Nuclear Engineering and Design*. Festschrift Edition Celebrating the 65th Birthday of Prof. Richard T. Lahey, Jr. 235.10 (May 1, 2005), pp. 1149–1161. ISSN: 0029-5493. DOI: [10.1016/j.nucengdes.2005.02.012](https://doi.org/10.1016/j.nucengdes.2005.02.012).
- [92] Tomio Okawa, Kazuhiro Kaiho, Shintaro Sakamoto, and Koji Enoki. "Observation and modelling of bubble dynamics in isolated bubble regime in subcooled flow boiling". In: *Nuclear Engineering and Design* 335 (Aug. 15, 2018), pp. 400–408. ISSN: 0029-5493. DOI: [10.1016/j.nucengdes.2018.06.009](https://doi.org/10.1016/j.nucengdes.2018.06.009).
- [93] M. S. Plesset and S. A. Zwick. "The Growth of Vapor Bubbles in Superheated Liquids". In: *Journal of Applied Physics* 25.4 (Apr. 1954). Number: 4, pp. 493–450. ISSN: 0021-8979.
- [94] Michael Z. Podowski and Raf M. Podowski. "Mechanistic Multidimensional Modeling of Forced Convection Boiling Heat Transfer". In: *Science and Technology of Nuclear Installations* 2009 (Dec. 22, 2008). Publisher: Hindawi, e387020. ISSN: 1687-6075. DOI: [10.1155/2009/387020](https://doi.org/10.1155/2009/387020).
- [95] V Prodanovic, D Fraser, and M Salcudean. "Bubble behavior in subcooled flow boiling of water at low pressures and low flow rates". In: *International Journal of Multiphase Flow* 28.1 (Jan. 1, 2002), pp. 1–19. ISSN: 0301-9322. DOI: [10.1016/S0301-9322\(01\)00058-1](https://doi.org/10.1016/S0301-9322(01)00058-1).
- [96] W. E. Ranz. "Evaporation from drops". In: *Chemical Engineering Progress* (Jan. 1, 1952). ISSN: 0360-7275.
- [97] Lord Rayleigh. "VIII. On the pressure developed in a liquid during the collapse of a spherical cavity". In: *The London, Edinburgh, and Dublin Philosophical Magazine and Journal of Science* 34.200 (Aug. 1, 1917). Publisher: Taylor & Francis _eprint: <https://doi.org/10.1080/14786440808635681>, pp. 94–98. ISSN: 1941-5982. DOI: [10.1080/14786440808635681](https://doi.org/10.1080/14786440808635681).
- [98] H. Reichardt. "Vollständige Darstellung der turbulenten Geschwindigkeitsverteilung in glatten Leitungen". In: *Zeitschrift Angewandte Mathematik und Mechanik* 31 (Jan. 1, 1951). ADS Bibcode: 1951ZaMM...31..208R, pp. 208–219. ISSN: 0044-2267. DOI: [10.1002/zamm.19510310704](https://doi.org/10.1002/zamm.19510310704).
- [99] Tingting Ren, Zhiqiang Zhu, Rui Zhang, Jiangwu Shi, and Changqi Yan. "Development of force balance model for prediction of bubble departure diameter and lift-off diameter in subcooled flow boiling". In: *International Journal of Heat and Mass Transfer* 161 (Nov. 1, 2020), p. 120245. ISSN: 0017-9310. DOI: [10.1016/j.ijheatmasstransfer.2020.120245](https://doi.org/10.1016/j.ijheatmasstransfer.2020.120245).
- [100] Andrew Jonathan Richenderfer. "Experimental study of heat flux partitioning in pressurized subcooled flow boiling". Accepted: 2018-11-15T15:51:52Z. Thesis. Massachusetts Institute of Technology, 2018.

- [101] Andrew Richenderfer, Artyom Kossolapov, Jee Hyun Seong, Giacomo Saccone, Etienne Demarly, Ravikishore Kommajosyula, Emilio Baglietto, Jacopo Buongiorno, and Matteo Bucci. "Investigation of subcooled flow boiling and CHF using high-resolution diagnostics". In: *Experimental Thermal and Fluid Science* 99 (Dec. 1, 2018), pp. 35–58. ISSN: 0894-1777. DOI: [10.1016/j.expthermflusci.2018.07.017](https://doi.org/10.1016/j.expthermflusci.2018.07.017).
- [102] E. Ruckenstein. "On mass transfer in the continuous phase from spherical bubbles or drops". In: *Chemical Engineering Science* 19.2 (Feb. 1, 1964), pp. 131–146. ISSN: 0009-2509. DOI: [10.1016/0009-2509\(64\)85117-4](https://doi.org/10.1016/0009-2509(64)85117-4).
- [103] Pierre Ruyer and Nathalie Seiler. "Modélisation avancée de la polydispersion en taille des écoulements bouillants". In: *La Houille Blanche* 4 (Aug. 1, 2009). Number: 4 Publisher: EDP Sciences, pp. 65–71. ISSN: 0018-6368, 1958-5551. DOI: [10.1051/lhb/2009046](https://doi.org/10.1051/lhb/2009046).
- [104] P. G. Saffman. "The lift on a small sphere in a slow shear flow". In: *Journal of Fluid Mechanics* 22.2 (June 1965), pp. 385–400. ISSN: 0022-1120, 1469-7645. DOI: [10.1017/S0022112065000824](https://doi.org/10.1017/S0022112065000824).
- [105] V. Scheiff, F. Bergame, J. Sebilleau, P. Ruyer, and C. Colin. "Experimental study of steady and transient subcooled flow boiling". In: *International Journal of Heat and Mass Transfer* 164 (Jan. 1, 2021), p. 120548. ISSN: 0017-9310. DOI: [10.1016/j.ijheatmasstransfer.2020.120548](https://doi.org/10.1016/j.ijheatmasstransfer.2020.120548).
- [106] Valentin Scheiff. "Etude expérimentale et modélisation du transfert de chaleur de l'ébullition transitoire". These de doctorat. Toulouse, INPT, Dec. 13, 2018.
- [107] L. E. Scriven. "On the dynamics of phase growth". In: *Chemical Engineering Science* 10.1 (Apr. 1, 1959), pp. 1–13. ISSN: 0009-2509. DOI: [10.1016/0009-2509\(59\)80019-1](https://doi.org/10.1016/0009-2509(59)80019-1).
- [108] Pengyu Shi, Roland Rzehak, Dirk Lucas, and Jacques Magnaudet. "Drag and lift forces on a rigid sphere immersed in a wall-bounded linear shear flow". In: *Physical Review Fluids* 6.10 (Oct. 28, 2021). Number: 10 Publisher: American Physical Society, p. 104309. ISSN: 2469-990X.
- [109] Rong Situ, Takashi Hibiki, Mamoru Ishii, and Michitsugu Mori. "Bubble lift-off size in forced convective subcooled boiling flow". In: *International Journal of Heat and Mass Transfer* 48.25 (Dec. 1, 2005), pp. 5536–5548. ISSN: 0017-9310. DOI: [10.1016/j.ijheatmasstransfer.2005.06.031](https://doi.org/10.1016/j.ijheatmasstransfer.2005.06.031).
- [110] Jia-Wen Song and Li-Wu Fan. "Temperature dependence of the contact angle of water: A review of research progress, theoretical understanding, and implications for boiling heat transfer". In: *Advances in Colloid and Interface Science* 288 (Feb. 1, 2021), p. 102339. ISSN: 0001-8686. DOI: [10.1016/j.cis.2020.102339](https://doi.org/10.1016/j.cis.2020.102339).
- [111] Charles G. Speziale, Sutanu Sarkar, and Thomas B. Gatski. "Modelling the pressure-strain correlation of turbulence: an invariant dynamical systems approach". In: *Journal of Fluid Mechanics* 227 (June 1991). Publisher: Cambridge University Press, pp. 245–272. ISSN: 1469-7645, 0022-1120. DOI: [10.1017/S0022112091000101](https://doi.org/10.1017/S0022112091000101).
- [112] R. Sugrue and J. Buongiorno. "A modified force-balance model for prediction of bubble departure diameter in subcooled flow boiling". In: *Nuclear Engineering and Design* 305 (Aug. 15, 2016), pp. 717–722. ISSN: 0029-5493. DOI: [10.1016/j.nucengdes.2016.04.017](https://doi.org/10.1016/j.nucengdes.2016.04.017).
- [113] R. Sugrue, J. Buongiorno, and T. McKrell. "An experimental study of bubble departure diameter in subcooled flow boiling including the effects of orientation angle, subcooling, mass flux, heat flux, and pressure". In: *Nuclear Engineering and Design*. SI : CFD4NRS-4 279 (Nov. 1, 2014), pp. 182–188. ISSN: 0029-5493. DOI: [10.1016/j.nucengdes.2014.08.009](https://doi.org/10.1016/j.nucengdes.2014.08.009).
- [114] Rosemary M. Sugrue. "The Effects of Orientation Angle, Subcooling, Heat Flux, Mass Flux, and Pressure on Bubble Growth and Detachment in Subcooled Flow Boiling". PhD thesis. Massachusetts Institute of Technology, 2012.
- [115] M. Sultan and R. L. Judd. "Spatial Distribution of Active Sites and Bubble Flux Density". In: *Journal of Heat Transfer* 100.1 (Feb. 1, 1978), pp. 56–62. ISSN: 0022-1481. DOI: [10.1115/1.3450504](https://doi.org/10.1115/1.3450504).
- [116] J. R. S. Thom, W. M. Walker, T. A. Fallon, and G. F. S. Reising. "Boiling In Sub-Cooled Water During Flow Up Heated Tubes or Annuli." In: *Proc. Inst. Mech. Eng. (London)*, 180: Pt 3C, 226-46(1965-66). (Oct. 31, 1967). Institution: Babcock and Wilcox Ltd., Renfrew, Eng.

- [117] G. E. Thorncroft, J. F. Klausner, and R. Mei. "An experimental investigation of bubble growth and detachment in vertical upflow and downflow boiling". In: *International Journal of Heat and Mass Transfer* 41.23 (Dec. 1, 1998), pp. 3857–3871. ISSN: 0017-9310. DOI: [10.1016/S0017-9310\(98\)00092-1](https://doi.org/10.1016/S0017-9310(98)00092-1).
- [118] G.E. Thorncroft, J.F. Klausner, and R. Mei. "Bubble forces and detachment models". In: *Multiphase Science and Technology* 13.3 (2001), pp. 35–76. ISSN: 0276-1459. DOI: [10.1615/multscientechn.v13.i3-4.20](https://doi.org/10.1615/multscientechn.v13.i3-4.20).
- [119] V. I. Tolubinsky and D. M. Kostanchuk. "VAPOUR BUBBLES GROWTH RATE AND HEAT TRANSFER INTENSITY AT SUBCOOLED WATER BOILING". In: International Heat Transfer Conference 4. Begel House Inc., 1970. DOI: [10.1615/IHTC4.250](https://doi.org/10.1615/IHTC4.250).
- [120] Akio Tomiyama, Hidesada Tamai, Iztok Zun, and Shigeo Hosokawa. "Transverse migration of single bubbles in simple shear flows". In: *Chemical Engineering Science* 57.11 (June 1, 2002), pp. 1849–1858. ISSN: 0009-2509. DOI: [10.1016/S0009-2509\(02\)00085-4](https://doi.org/10.1016/S0009-2509(02)00085-4).
- [121] G. G. Treshchev. "The number of vapor-formation centers in surface boiling". In: *Convective Heat Transfer in Two-Phase and One-Phase Flows*. Borishanskii V.M. and Paleev I.I. Jerusalem: Israel Program for Scientific Translations, 1969, pp. 97–105.
- [122] A. Urbano, S. Tanguy, and C. Colin. "Direct numerical simulation of nucleate boiling in zero gravity conditions". In: *International Journal of Heat and Mass Transfer* 143 (Nov. 1, 2019), p. 118521. ISSN: 0017-9310. DOI: [10.1016/j.ijheatmasstransfer.2019.118521](https://doi.org/10.1016/j.ijheatmasstransfer.2019.118521).
- [123] A. Urbano, S. Tanguy, G. Huber, and C. Colin. "Direct numerical simulation of nucleate boiling in micro-layer regime". In: *International Journal of Heat and Mass Transfer* 123 (Aug. 1, 2018), pp. 1128–1137. ISSN: 0017-9310. DOI: [10.1016/j.ijheatmasstransfer.2018.02.104](https://doi.org/10.1016/j.ijheatmasstransfer.2018.02.104).
- [124] W. G. J. Van Helden, C. W. M. Van Der Geld, and P. G. M. Boot. "Forces on bubbles growing and detaching in flow along a vertical wall". In: *International Journal of Heat and Mass Transfer* 38.11 (July 1, 1995), pp. 2075–2088. ISSN: 0017-9310. DOI: [10.1016/0017-9310\(94\)00319-Q](https://doi.org/10.1016/0017-9310(94)00319-Q).
- [125] L. Van Wijngaarden and D. J. Jeffrey. "Hydrodynamic interaction between gas bubbles in liquid". In: *Journal of Fluid Mechanics* 77.1 (Sept. 1976). Publisher: Cambridge University Press, pp. 27–44. ISSN: 1469-7645, 0022-1120. DOI: [10.1017/S0022112076001110](https://doi.org/10.1017/S0022112076001110).
- [126] G. H. Yeoh, Sherman C. P. Cheung, J. Y. Tu, and Mark K. M. Ho. "Fundamental consideration of wall heat partition of vertical subcooled boiling flows". In: *International Journal of Heat and Mass Transfer* 51.15 (July 15, 2008), pp. 3840–3853. ISSN: 0017-9310. DOI: [10.1016/j.ijheatmasstransfer.2007.11.047](https://doi.org/10.1016/j.ijheatmasstransfer.2007.11.047).
- [127] Junsoo Yoo, Carlos E. Estrada-Perez, and Yassin A. Hassan. "Experimental study on bubble dynamics and wall heat transfer arising from a single nucleation site at subcooled flow boiling conditions – Part 1: Experimental methods and data quality verification". In: *International Journal of Multiphase Flow* 84 (Sept. 1, 2016), pp. 315–324. ISSN: 0301-9322. DOI: [10.1016/j.ijmultiphaseflow.2016.04.018](https://doi.org/10.1016/j.ijmultiphaseflow.2016.04.018).
- [128] Junsoo Yoo, Carlos E. Estrada-Perez, and Yassin A. Hassan. "Experimental study on bubble dynamics and wall heat transfer arising from a single nucleation site at subcooled flow boiling conditions – Part 2: Data analysis on sliding bubble characteristics and associated wall heat transfer". In: *International Journal of Multiphase Flow* 84 (Sept. 1, 2016), pp. 292–314. ISSN: 0301-9322. DOI: [10.1016/j.ijmultiphaseflow.2016.04.019](https://doi.org/10.1016/j.ijmultiphaseflow.2016.04.019).
- [129] Junsoo Yoo, Carlos E. Estrada-Perez, and Yassin A. Hassan. "Area of bubble influence due to sliding bubbles in subcooled boiling flow". In: *International Journal of Heat and Mass Transfer* 125 (Oct. 1, 2018), pp. 43–52. ISSN: 0017-9310. DOI: [10.1016/j.ijheatmasstransfer.2018.04.058](https://doi.org/10.1016/j.ijheatmasstransfer.2018.04.058).
- [130] Junsoo Yoo, Carlos E. Estrada-Perez, and Yassin A. Hassan. "Development of a mechanistic model for sliding bubbles growth prediction in subcooled boiling flow". In: *Applied Thermal Engineering* 138 (June 25, 2018), pp. 657–667. ISSN: 1359-4311. DOI: [10.1016/j.applthermaleng.2018.04.096](https://doi.org/10.1016/j.applthermaleng.2018.04.096).
- [131] Byong-Jo Yun, Andrew Splawski, Simon Lo, and Chul-Hwa Song. "Prediction of a subcooled boiling flow with advanced two-phase flow models". In: *Nuclear Engineering and Design*. SI : CFD4NRS-3 253 (Dec. 1, 2012), pp. 351–359. ISSN: 0029-5493. DOI: [10.1016/j.nucengdes.2011.08.067](https://doi.org/10.1016/j.nucengdes.2011.08.067).

- [132] L. Z. Zeng, J. F. Klausner, D. M. Bernhard, and R. Mei. “A unified model for the prediction of bubble detachment diameters in boiling systems—II. Flow boiling”. In: *International Journal of Heat and Mass Transfer* 36.9 (Jan. 1, 1993), pp. 2271–2279. ISSN: 0017-9310. DOI: [10.1016/S0017-9310\(05\)80112-7](https://doi.org/10.1016/S0017-9310(05)80112-7).
- [133] Lanying Zeng, Fady Najjar, S. Balachandar, and Paul Fischer. “Forces on a finite-sized particle located close to a wall in a linear shear flow”. In: *Physics of Fluids* 21.3 (Mar. 2009). Publisher: American Institute of Physics, p. 033302. ISSN: 1070-6631. DOI: [10.1063/1.3082232](https://doi.org/10.1063/1.3082232).
- [134] Pei Zhou, Shiyang Hua, Cai Gao, Dongfang Sun, and Ronghua Huang. “A mechanistic model for wall heat flux partitioning based on bubble dynamics during subcooled flow boiling”. In: *International Journal of Heat and Mass Transfer* 174 (Aug. 1, 2021), p. 121295. ISSN: 0017-9310. DOI: [10.1016/j.ijheatmasstransfer.2021.121295](https://doi.org/10.1016/j.ijheatmasstransfer.2021.121295).
- [135] Pei Zhou, Ronghua Huang, Sheng Huang, Yu Zhang, and Xiaoxuan Rao. “Experimental investigation on active nucleation site density and bubble departure frequency in subcooled flow boiling by using bubble tracking algorithm”. In: *International Journal of Heat and Mass Transfer* 148 (Feb. 1, 2020), p. 119081. ISSN: 0017-9310. DOI: [10.1016/j.ijheatmasstransfer.2019.119081](https://doi.org/10.1016/j.ijheatmasstransfer.2019.119081).
- [136] Pei Zhou, Ronghua Huang, Sheng Huang, Yu Zhang, and Xiaoxuan Rao. “Experimental investigation on bubble contact diameter and bubble departure diameter in horizontal subcooled flow boiling”. In: *International Journal of Heat and Mass Transfer* 149 (Mar. 1, 2020), p. 119105. ISSN: 0017-9310. DOI: [10.1016/j.ijheatmasstransfer.2019.119105](https://doi.org/10.1016/j.ijheatmasstransfer.2019.119105).
- [137] N. Zuber. “On the dispersed two-phase flow in the laminar flow regime”. In: *Chemical Engineering Science* 19.11 (Nov. 1, 1964), pp. 897–917. ISSN: 0009-2509. DOI: [10.1016/0009-2509\(64\)85067-3](https://doi.org/10.1016/0009-2509(64)85067-3).
- [138] Novak Zuber. “The dynamics of vapor bubbles in nonuniform temperature fields”. In: *International Journal of Heat and Mass Transfer* 2.1 (Mar. 1, 1961), pp. 83–98. ISSN: 0017-9310. DOI: [10.1016/0017-9310\(61\)90016-3](https://doi.org/10.1016/0017-9310(61)90016-3).
- [139] H. C. Ünal. “Maximum bubble diameter, maximum bubble-growth time and bubble-growth rate during the subcooled nucleate flow boiling of water up to 17.7 MN/m²”. In: *International Journal of Heat and Mass Transfer* 19.6 (June 1, 1976), pp. 643–649. ISSN: 0017-9310. DOI: [10.1016/0017-9310\(76\)90047-8](https://doi.org/10.1016/0017-9310(76)90047-8).